Forcing statistics in resolvent analysis: application in minimal turbulent Couette flow

Petrônio A. S. Nogueira[1], Pierluigi Morra[2], Eduardo Martini[1], André V. G. Cavalieri[1] and Dan S. Henningson[2]

[1]Instituto Tecnológico de Aeronáutica, Aerodynamics Department, São José dos Campos, 12228900, Brazil
[2]KTH Royal Institute of Technology, Dept. of Engineering Mechanics, FLOW, SE-10044, Stockholm, Sweden

Submitted to Journal of Fluid Mechanics

An analysis of the statistics of the non-linear terms in resolvent analysis is performed in this work for turbulent Couette flow at Reynolds number 400. Data from a direct numerical simulation of a minimal flow unit is post-processed using Fourier analysis in both time and space, leading to the covariance matrix of the velocity. From the same data, we computed the non-linear terms of the Navier-Stokes equations (treated as forcing in the present formulation), which allowed us to compute the covariance matrix of the forcing for this case. The two covariances are related exactly by the resolvent operator. Such a quantitative relation is confirmed here for the first time, accounting for relevant signal processing issues related to the windowing procedure for frequency-domain quantities. Such exact correspondence allowed the eduction of the most relevant force components. This is carried out for the dominant structures in this flow, which participate in the self-sustaining cycle of turbulence: (i) streamwise vortices and streaks, and (ii) spanwise-coherent fluctuations of spanwise velocity. The present results show a dominance by a subset of the non-linear terms for the prediction of the full statistics of streamwise vortices and streaks; a single term is seen to be dominant for spanwise motions. A relevant feature observed in these cases is that the forcing covariance is dominated by its first eigenfunction, showing that non-linear terms also have a coherent structure. Different forcing components are also coherent between them, which leads to constructive and destructive interferences that greatly modify the flow response. These observations show that forcing colour is an important feature of turbulent flows, and should thus be accounted for in modelling work.

---

1. Introduction

Coherent structures have been studied in turbulent flows for some time now. Findings in that area led to a change in view: instead of considering turbulence as completely stochastic, this is now seen as having a clear coherent motion among

the apparent unsteady, chaotic field. In turbulent jets, for instance, structures governed by the Kelvin-Helmholtz instability were found to be important not only for transition (Michalke 1964), but also for the sound radiation at shallow angles (Cavalieri *et al.* 2012). In wall-bounded flows, streamwise elongated, spanwise organised structures (called streaks), found firstly by Kline *et al.* (1967), are also ubiquitous in shear flows. These structures are found for all kinds of turbulent shear flows, including channels (Gustavsson 1991), pipes (Hellström *et al.* 2011), and even round jets (Nogueira *et al.* 2019).

The mechanism behind streak formation was firstly studied by Ellingsen & Palm (1975), later complemented by Landahl (1980). In their study, they concluded that the presence of shear in the mean flow and a non-zero wall-normal velocity induce momentum transfer between different layers of the fluid. If streamwise vortices are present, for instance, these generate streaks via a non-modal, linear mechanism such that, when fluid is lifted from high- to low-speed regions of the flow, a high-speed streak is formed (the opposite happening for a low-speed streak). This is called the lift-up effect and, considering that streaks are present in several shear flows, this effect should be an important part of the turbulent dynamics. This is explored, for example, by Hamilton *et al.* (1995); Waleffe (1997) where a self-sustaining process for wall bounded turbulence was proposed. This can be summarised as following: (i) streamwise vortices in the turbulent medium generate streamwise streaks via the lift-up effect; (ii) streaks grow until the instability is triggered, leading to their breakdown; (iii) the resulting flow interacts non-linearly in order to regenerate the streamwise vortices, thus restarting the process. The first step is well understood, and was considered by the work of Ellingsen & Palm (1975). The other stages have also received a good deal of attention: the streak breakdown was studied by Schoppa & Hussain (1999) using numerical simulation and linear stability theory, revealing that the breakdown of a low-speed streak directly generates new streamwise vortices in the end of the process. This was further explored numerically (Jiménez & Pinelli 1999; Andersson *et al.* 2001), experimentally (Asai *et al.* 2002) and even theoretically (Kawahara *et al.* 2003), using a simplified vortex sheet model. As synthesised by Brandt (2007), this process can occur via either a varicose or a sinuous mode, the latter being the dominant mechanism; in both cases, the final structures resulting from the instability of a low-speed streak are elongated in the streamwise direction (quasi-streamwise vortices).

The cited works focused on the steps leading to the breakdown of streaks, looking at the self-sustaining cycle in the time domain (in order to evaluate the sequence of events); in most cases results confirm qualitatively trends observed in turbulent flows, but quantitative comparisons are difficult due to the simplifications introduced in the modelling process. Alternative approaches for studying these phenomena are based on the analysis of the linearised Navier-Stokes operator, considering the mean field as the base flow. In this framework, linear methods such as resolvent analysis (Jovanovic & Bamieh 2005; McKeon & Sharma 2010) and linear transient growth (Butler & Farrell

1992; Schmid & Henningson 2001) are useful to obtain optimal responses from the harmonically forced linearised Navier-Stokes system (resolvent) or the flow structure resulting from a non-modal growth of initial disturbances (linear transient growth). Both analyses, albeit linear, reproduce some experimental trends in both wall-bounded flows (Del Alamo & Jimenez 2006; Pujals *et al.* 2009; Cossu *et al.* 2009; Sharma & McKeon 2013; Morra *et al.* 2019; Abreu *et al.* 2019) and free-shear flows (Schmidt *et al.* 2018; Lesshafft *et al.* 2019). Nevertheless, there are intrinsic limitations to these approaches. For instance, resolvent analysis typically considers the unknown forcing terms as spatially white noise, suggesting that the energetic coherent structures in the turbulent flow should be closely related to optimal response modes from resolvent (Towne *et al.* 2018*a*). Usually, this analysis assumes that the statistics of the non-linear terms are uncorrelated in space (spatial white noise), often due to lack of knowledge of the real force statistics. This assumption is never verified in practice, considering, for instance, that non-linear terms are zero on a wall, and should be negligible in regions of uniform flow. Moreover, non-linear terms are expected to have a specific structure, as they result from the turbulent flow field which itself has a level of organization.

Hence, attempts have been made to identify the colour of such "forcing" terms using some flow statistics. Zare *et al.* (2017), for instance, proposed a formulation to estimate the non-linear forcing statistics from a turbulent flow field based on the knowledge of a limited number of velocity correlations. Similar work was performed by Towne *et al.* (2020), who proposed a method for estimating the systems response statistics via an indirect estimation of the system force statistic, although a comparison between the estimated and real forces is not presented. The method was applied to different problems, such as Ginzburg-Landau and linearised Navier-Stokes, showing that it can outperform several approaches in flow cases that are not dominated by the first resolvent mode. It is worth noting that the cited works focused on estimating the forcing from a limited number of sensors, in an optimisation framework aimed at matching statistics from such sensors, instead of evaluating the characteristics of such forcing. Also, there is thus no *a priori* guarantee that the identified forcing is the one actually present in turbulence dynamics. In his thesis, Towne (2016) also analysed the structure of the equivalent non-linear forcing of a turbulent jet using data from a large-eddy simulation. The preliminary results of forcing, as computed in the cited work, can be considered as a first approximation of the non-linear terms of the Navier-Stokes equations; still, it also accounts for the subgrid model in the simulation. This earlier effort did not account for windowing issues later studied by Martini *et al.* (2019), and hence the presented results may suffer from signal processing issues. Another way to consider the structure of non-linear terms is by introducing an eddy viscosity model on the linearised Navier-Stokes operators (Del Alamo & Jimenez 2006; Pujals *et al.* 2009; Illingworth *et al.* 2018; Morra *et al.* 2019), which models at least part of non-linear effects as turbulent diffusion on the flow structures. However, such

model should not be required when full force knowledge is available and the proper signal treatment is performed.

None of the cited works dealt with the exact covariance, within numerical accuracy, of non-linear terms, as each included some degree of approximation whose effect is difficult to evaluate *a priori*. In order to avoid the simplifications above, one may consider the exact covariance of the non-linear terms in the analysis. By taking the exact covariance of the non-linear terms into account (or the cross-spectral density if the analysis is carried out in the frequency domain), the exact response of the system can be obtained. To the best of the authors' knowledge, this has not been attempted for turbulent flows, but only for model problems such as the forced Ginzburg-Landau equation (Towne *et al.* 2018*a*; Cavalieri *et al.* 2019). A notable exception is the work of Chevalier *et al.* (2006), where time covariances of the non-linear terms are obtained from a simulation of turbulent channel flow, and subsequently used, assuming white noise in time, to design estimators of flow fluctuations using Kalman filters. However, the use of the exact covariance of the non-linear forcing term can be prohibitive for complex flow cases. Therefore, an approximation or modelling of the forcing term is usually needed to reduce the number of variables to be computed/modelled, and may also lead to insight on the relevant physics, as the dominant mechanisms of excitation of flow structures may be thus isolated. An analysis of forcing covariances should reveal the degree of organisation of the excitation, showing how significant are the departures from the simplified white-noise assumption.

This work focuses on the analysis of the non-linear forcing term in the resolvent analysis of a turbulent Couette flow, here studied in the minimal computational box of Hamilton *et al.* (1995), which allows a full determination of the cross-spectral densities of forcing and response without any simplifying assumption. Differently from other previous approaches (Zare *et al.* 2017; Towne *et al.* 2020), instead of estimating the forcing from a subset of data in order to estimate other flow statistics, we explicitly compute the non-linear term of the Navier-Stokes equations, performing the whole analysis using the actual statistics of these terms. Reduction of the complexity of forcing statistics can be performed subsequently in modelling steps, whose accuracy may be evaluated by computing flow responses to simplified forcings using the resolvent operator. The paper is divided as follows: In § 2 the relevant parameters of the simulation are defined, followed by the methods showing how the covariance of the velocity fluctuations is obtained from the covariance of the non-linear terms of the Navier-Stokes equations. The reconstruction of the velocity statistics from the forcing covariance is evaluated in § 3, where the role of the windowing correction term is highlighted. After that, in § 4 we focus on obtaining the relevant parts of the non-linear terms (the ones that will generate the bulk of the covariance of the response) for two different cases (streaks, and streamwise oscillations of spanwise velocity). The paper closes in § 5 with a connection between this analysis and the self-sustaining cycle characteristic of turbulent Couette flow.

2. Numerical approach

The case chosen for the study is the Couette flow in the minimal flow unit. Such a flow case retains salient features of turbulent flows, like the dominance of streaks by the lift-up effect and the self-sustaining process defined by Hamilton *et al.* (1995); Waleffe (1997), and minimises computational power requirements.

2.1. *The Minimal Flow Unit*

The flow case chosen is the one explored by Hamilton *et al.* (1995). It is defined by the smallest box and the smallest Reynolds number in which turbulence can be sustained without any external forcing. For Couette flow, the minimal box has dimensions $(L_x, L_y, L_z) = (1.75\pi h, 2h, 1.2\pi h)$, denoting lengths in the streamwise, wall-normal and spanwise directions, respectively; h is the channel half-height. The discretisation was chosen as $(n_x, n_y, n_z) = (32, 65, 32)$ before dealiasing in the wall-parallel directions, which gives a slightly higher resolution than the one used in Hamilton *et al.* (1995). We consider Couette flow with walls moving at velocity $\pm U_w$; the Reynolds number for this case is $Re = 400$, based on wall velocity U_w and half-height h. For this flow this leads to a friction Reynolds number $Re_\tau \approx 34$, based on the friction velocity. From now on, all quantities are non-dimensional values based on outer units, with h and U_w as reference length and velocity. The simulation is performed in SIMSON, a pseudo-spectral solver for incompressible flows (Chevalier *et al.* 2007), with discretisation in Fourier modes in streamwise and spanwise directions, and in Chebyshev polynomials in the wall-normal direction.

The simulation is initialised with white noise in space for $Re = 625$, which becomes turbulent after a few timesteps; the Reynolds number is, then, slowly decreased until the desired value of 400. After reaching the desired value of Re and discarding initial transients, flow fields are stored every $\Delta t = 0.5$ in the interval $10000 < t < 25000$. During this period, several streak regeneration cycles are observed, and the flow is expected to be statistically stationary. The mean turbulent velocity profile is shown in figure 1(a), which has the usual "S" profile typical of turbulent Couette flow. The mean profile and fluctuation levels match previous results for the same computational domain and Reynolds number (Gibson *et al.* 2008). A snapshot of the streamwise velocity fluctuations for a (y, z) plane is shown in figure 1(b). As expected, streaks arise clearly in the velocity field, since these structures are the most relevant in the turbulent dynamics of this sheared flow; they are flanked by streamwise vortices with the expected lift-up behaviour: positions with downward/upward motion display lifted high/low momentum, leading to a high/low-speed streak.

Using the results from the DNS, the velocity fluctuations around the mean flow profile (treated as response of the input-output version of the Navier-Stokes system) were computed; these, in turn, were used to compute the non-linear terms of the Navier-Stokes equations, which will be treated as a forcing term in the N-S equations expanded around the mean flow. These are computed directly as a function of time in the physical domain. After that, the resulting forcing

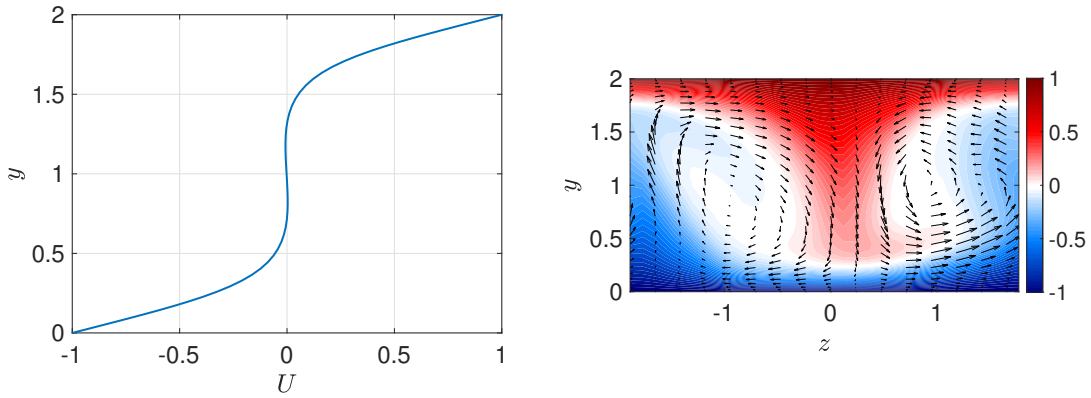

(a) Mean flow

(b) Snapshot of velocity field

Figure 1: Mean velocity for Couette flow and snapshot of the velocity field in the (y, z) plane (colours: streamwise velocity; arrows: spanwise and wall-normal velocities).

was Fourier transformed in space, leading to forcings as a function of streamwise and spanwise wavenumbers, but still in the time domain. Using the forcing and velocity in the time-wavenumber domain, we computed the cross-spectral densities of the response (**S**) and of the forcing (**P**). This is further detailed in the next section.

2.2. *Recovering response statistics from the forcing cross-spectral density*

Since Couette flow is homogeneous in x and z directions, the first step for the analysis of this flow is to perform a spatial Fourier transform of both response and forcing, so the analysis can be performed separately for each wavenumber. Modes are defined by the integers (n_α, n_β), with $\alpha = 2\pi n_\alpha / L_x$ and $\beta = 2\pi n_\beta / L_z$ being the wavenumbers, following the same notation of Hamilton *et al.* (1995). The wall-normal integrated kinetic energy of the first two modes, some of the most relevant ones in the analysis of Hamilton *et al.* (1995), is shown in figure 2, showing the fluctuations peak at vanishing frequency $\omega \to 0$ for mode $(0, 1)$, and a plateau is observed at low frequencies for mode $(1, 0)$. Since we consider a Couette flow with walls moving at opposite velocities, $\pm U_w$, this very-low frequency behaviour reflects that the two modes peak at approximately zero phase speed, without preferred motion following some streamwise or spanwise direction, as can be induced from the results of Hamilton *et al.* (1995). The time power spectral density (PSD) for each mode was estimated using the Welch method, with the signal divided in segments of $n_{fft} = 1024$ with 75% overlap, which led to 114 blocks for the analysis. A Hanning window was used to reduce spectral leakage, allowing accurate relation between forcing and response of the system.

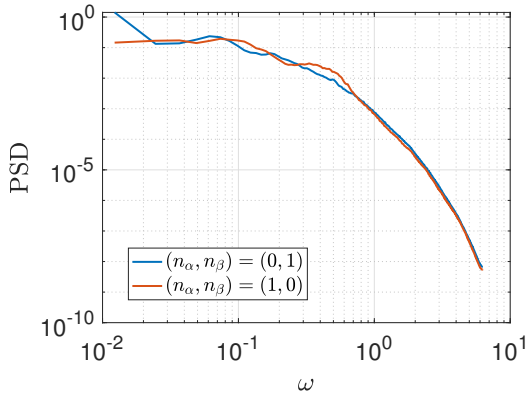

Figure 2: Power spectral density of the wall-normal integrated kinetic energy for the different modes studied herein.

We will study the two most energetic modes at low frequencies, as showed in Hamilton *et al.* (1995): mode $(0, 1)$, which is related to the appearance of streaks; and mode $(1, 0)$, which emerge once the amplitude of mode $(0, 1)$ decreases, characterising streak breakdown (Hamilton *et al.* 1995). Applying the Reynolds decomposition, we will consider an expansion around the mean flow, averaged over streamwise and spanwise directions and in time, so that each component of the velocity can be written as the sum of mean and fluctuation fields $(U_i + \tilde{u}_i)$, with U_i denoting the mean velocity profile and the tilde indicating fluctuations in time domain. Thus, we can write the incompressible Navier-Stokes equations as

$$\frac{\partial \tilde{u}_i}{\partial t} + U_j \frac{\partial \tilde{u}_i}{\partial x_j} + \tilde{u}_j \frac{\partial U_i}{\partial x_j} = -\frac{\partial \tilde{p}}{\partial x_i} + \frac{1}{Re} \frac{\partial^2 \tilde{u}_i}{\partial x_j \partial x_j} + \tilde{f}_i, \tag{1}$$

and the continuity equation

$$\frac{\partial \tilde{u}_i}{\partial x_i} = 0, \tag{2}$$

where Einstein summation is implied, $\tilde{u}_i$ are the three velocity components, $\tilde{p}$ is the pressure and the forcing term $\tilde{f}_i$ is considered to gather the non-linear terms of the Navier-Stokes equations,

$$\tilde{f}_i = -\tilde{u}_j \partial \tilde{u}_i / \partial x_j + \overline{\tilde{u}_j \partial \tilde{u}_i / \partial x_j}. \tag{3}$$

where $\overline{\tilde{u}_j \partial \tilde{u}_i / \partial x_j}$ is the mean Reynolds stress, which is only be present in the zero-frequency/zero-wavenumber equation (i.e. the mean-flow equation, which is the Reynolds averaged Navier-Stokes equation). Taking the Fourier transform

in x, z and t, and considering that the mean flow has only the streamwise component $U(y)$, leads to

$$-\mathrm{i}\omega u + \mathrm{i}\alpha U u + v\frac{\partial U}{\partial y} = -\mathrm{i}\alpha p + \frac{1}{Re}\left(-\alpha^2 - \beta^2 + \frac{\partial^2}{\partial y^2}\right)u + f_x \tag{4a}$$

$$-\mathrm{i}\omega v + \mathrm{i}\alpha U v = -\frac{\partial p}{\partial y} + \frac{1}{Re}\left(-\alpha^2 - \beta^2 + \frac{\partial^2}{\partial y^2}\right)v + f_y \tag{4b}$$

$$-\mathrm{i}\omega w + \mathrm{i}\alpha U w = -\mathrm{i}\beta p + \frac{1}{Re}\left(-\alpha^2 - \beta^2 + \frac{\partial^2}{\partial y^2}\right)w + f_z \tag{4c}$$

$$\mathrm{i}\alpha u + \frac{\partial v}{\partial y} + \mathrm{i}\beta w = 0, \tag{4d}$$

where ω is the frequency, (u, v, w, p) are the Fourier transformed perturbation quantities, and (f_x, f_y, f_z) the Fourier transforms of $\tilde{f}_i$. From the equations above, we can write the incompressible Navier-Stokes equations for the perturbations in the wavenumber and frequency domain in an input-output form as

$$-\mathrm{i}\omega\mathbf{H}\mathbf{q} = \mathbf{A}\mathbf{q} + \mathbf{f}, \tag{5}$$

where $\mathbf{q} = [u\ v\ w\ p]^T$ is the output and $\mathbf{f} = [f_x\ f_y\ f_z\ 0]^T$ is the forcing term (input). The matrix $\mathbf{A}$ is the linear operator defined by Navier-Stokes and continuity equations (which is a function of the streamwise and spanwise wavenumbers α and β) and the matrix $\mathbf{H}$ is defined to zero the time derivative of the pressure. This can be rewritten in the usual resolvent form

$$(-\mathrm{i}\omega\mathbf{H} - \mathbf{A})\mathbf{q} = \mathbf{f} \tag{6}$$

$$\Rightarrow \mathbf{L}\mathbf{q} = \mathbf{f} \tag{7}$$

$$\Rightarrow \mathbf{q} = \mathbf{L}^{-1}\mathbf{f} = \mathbf{R}\mathbf{f}. \tag{8}$$

With the equations written in this shape, optimal forcings and responses (in the linear framework, based on linearisation of the Navier-Stokes equations around the mean flow) can be obtained for a turbulent flow by performing a singular value decomposition of the resolvent operator, which leads to orthogonal bases for responses $\mathbf{q}_i$ and forcings $\mathbf{f}_i$, related by gains s_i. In other words, resolvent analysis amounts to solving the linear optimisation problem given by

$$s_1^2 = \max_{\mathbf{f}} \frac{\langle \mathbf{R}\mathbf{f}, \mathbf{R}\mathbf{f} \rangle}{\langle \mathbf{f}, \mathbf{f} \rangle}, \tag{9}$$

where $\langle\ ,\ \rangle$ is the Euclidean inner product associated with the energy norm, and s_1 is the highest resolvent gain. The solution for equation 9 is obtained by performing a singular value decomposition of the resolvent operator $\mathbf{R}$. When inner products other than Euclidean are considered, eq. 9 is modified to account for weighting matrices related to forcing and response spaces, and such matrices

are used in the singular value decomposition; the reader is referred to Schmidt *et al.* (2018) for the complete description of the inclusion of weighting matrices. Here the same weighting matrix was used for both forcing and response spaces, corresponding to Clenshaw-Curtis quadrature associated with the Chebyshev weights in the present grid (Trefethen 2000).

Optimal response and the respective gain from resolvent analysis are directly comparable to the most energetic structures in the flow if the forcing is considered to be statistically white in space (Towne *et al.* 2018*a*). In order to consider the actual statistics of the flow in this framework, we define the covariance matrices of the response $\mathbf{S} = \mathcal{E}(qq^H)$ and of the forcing $\mathbf{P} = \mathcal{E}(ff^H)$, and $\mathcal{E}$ representing the expected value of a signal, which is computed by averaging realisations in the Welch method (taking the block-average of $\mathbf{qq}^H$ as a function of frequency). Following Towne *et al.* (2018*a*); Cavalieri *et al.* (2019), these quantities are related via

$$\begin{aligned} \mathbf{qq}^H &= \mathbf{R}\mathbf{ff}^H\mathbf{R}^H \\ \mathcal{E}(\mathbf{qq}^H) &= \mathbf{R}\mathcal{E}(\mathbf{ff}^H)\mathbf{R}^H \\ \mathbf{S} &= \mathbf{RPR}^H. \end{aligned} \tag{10}$$

If it is assumed that the covariance of the forcing is uncorrelated in space, then $\mathbf{P} = \mathrm{I}$ and the covariance of the response is given by $\mathbf{S} = \mathbf{RR}^H$. Therefore, if the statistics of the forcing follows this hypothesis, the SPOD modes, defined by the eigenfunctions of

$$\int_{-1}^{1} \mathbf{S}(y, y', \omega)\mathbf{q}_{SPOD}(y', \omega)\mathrm{d}y' = \sigma\mathbf{q}_{SPOD}(y, \omega) \tag{11}$$

are identical to response modes (left singular vectors of $\mathbf{R}$). For more details on this derivation, the reader should refer to Towne *et al.* (2018*a*); Cavalieri *et al.* (2019). As in the computation of resolvent modes, SPOD modes are computed numerically with the inclusion of integration weights (Schmidt *et al.* 2018), such that flow structures resulting from both analyses can be directly compared to each other.

However, non-white forcing covariance (which must be the case in turbulent flows) must be included in the formulation in order to correctly educe the response statistics. The inclusion of $\mathbf{P}$ can be done in several ways. One of them is to directly compute the non-linear terms of the Navier-Stokes equations from simulation data. Other approaches include modelling the forcing starting from specific assumptions on the flow case (Moarref *et al.* 2013), its identification from limited flow information (Zare *et al.* 2017; Towne *et al.* 2018*b*), and modelling by means of an eddy viscosity included in the linear operator (Tammisola & Juniper 2016; Morra *et al.* 2019).

The present work focuses on exploring different forcing covariances and their effect on the covariance of the response. The first approach is to simply consider

the forcing to be uncorrelated in space; for this case, previous analyses for wall-bounded flows has shown that even though reasonable agreement may be obtained for near-wall fluctuations (Abreu *et al.* 2019), a mismatch is observed for large-scale structures (Morra *et al.* 2019). One can also compute the non-linear terms directly from a numerical simulation and then determine accurately $\mathbf{P}$. If the simulation is converged and the signal processing is done properly, the result of equation 10 using the actual forcing covariance $\mathbf{P}$ (in the sense that this quantity is directly obtained from the simulation) should be equal to the response covariance $\mathbf{S}$ computed from the same simulation.

3. Reconstruction of response statistics from the full forcing CSD

3.1. *Connection between forcing and response statistics – role of the correction due to windowing*

Although equation 10 is exact, if $\mathbf{P}$ and $\mathbf{S}$ are estimated from a finite set of data, large errors arise in the velocity statistics recovery process using the resolvent operator, leading to non-negligible values for $\mathbf{S} - \mathbf{RPR}^H$. From the analysis of Martini *et al.* (2019) (summarised in Appendix A for the present case), application of windowing in the data (which is necessary for applying Welch's method) generates extra force-like terms that must be accounted to have the correct input-output relation, so that equation 10 holds for the estimated covariances. The impact of these extra terms can be measured as

$$Error = \frac{||\mathbf{S}_{rec} - \mathbf{S}||}{||\mathbf{S}||}, \tag{12}$$

where $\mathbf{S}_{rec}$ is the covariance of the response recovered from the statistics of the forcing using eq. 10, applied for both uncorrected and corrected forcing terms; the norm was chosen as the standard 2-norm for matrices. With this metric, we can evaluate how this correction term affects the process of recovering $\mathbf{S}$ from $\mathbf{P}$. The comparison of the errors with and without this correction term is shown in figure 3 for the two Fourier modes studied in this work.

From figure 3, we can see that the correction affects a wide range of frequencies, with a slightly lower effect in higher frequencies. Following Martini *et al.* (2019), we can divide the aliasing error into two components: the first is due to spectral content at frequencies higher than the Nyquist frequency, and the other is due to the window spectral leakage, which generates extra content above the Nyquist frequency. Only the latter can be reduced with a proper choice of windowing function. The aliasing behaviour of the error explain the larger errors obtained at higher frequencies in figure 3, and indicates that the first type of aliasing is dominant in that region. As this work will focus on the study of low frequency structures, no further effort is made in order to reduce the error in higher frequencies; moreover, since the normalised errors are below 10^{-4} in all cases, an optimisation of the window was deemed unnecessary for our purposes.

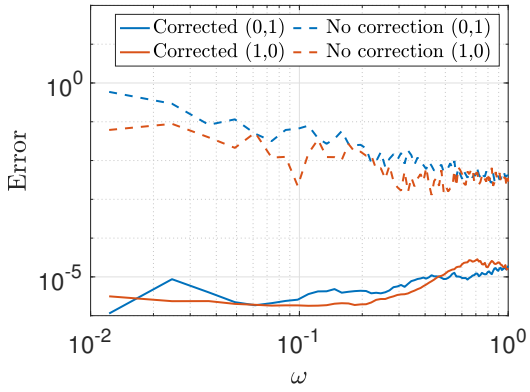

Figure 3: Effect of the correction term in the recovery of $\mathbf{S}$. Error spectrum normalised by $\Delta\omega$.

The correction greatly improves the recovery process for all modes, leading to a reduction of the error of about 5 orders of magnitude for the two considered modes, which is possibly related to the low-order dynamics of the flow for this combination of wavenumbers, a feature that will be further explored in §4.1 and 4.2. The effect of the correction on the shapes of each case will be studied in the next section.

The role of the forcing terms is studied throughout this work. All the comparisons between forces and responses will implicitly consider the correction term, unless otherwise stated. In all other contexts "external force" will refer only to the term $\mathbf{f}$, without considering the correction term.

3.2. *Comparison with statistics from white-noise forcing and no correction*

Here, we analyse the effect of the different choices of forcing CSD $\mathbf{P}$ on the velocity statistics. As stated previously, we focus on very low frequencies in order to evaluate the effect of the statistics of the non-linear terms on the most energetic streaks, and on the equivalent structures for other combinations of wavenumbers. For that reason, we choose $\omega = 0.0123$ for the analysis of modes $(0, 1)$ and $(1, 0)$; this is the first non-zero frequency from the Welch method for the present case (this frequency can be seen as the limit $\omega \to 0$ in this analysis). This frequency was chosen so as to analyse the behaviour of the very-large, almost time-invariant structures observed in the minimal flow unit. Analogous structures have been identified by a number of authors (Komminaho *et al.* 1996; Tsukahara *et al.* 2006; Pirozzoli *et al.* 2011, 2014; Lee & Moser 2018) for turbulent Couette flow at higher Reynolds numbers. For the present low Reynolds number, these large structures have the same characteristic length of the near-wall streaks; since they have the same overall behaviour, it becomes harder to separate these in such a small box. The analysis of Rawat *et al.* (2015) indicates nonetheless that the minimal flow unit streaks become very large scale structures in turbulent Couette flow if continuation methods are

applied. Therefore, the analysis of mode $(n_\alpha, n_\beta) = (0, 1)$ should be seen as a study of the overall dynamics of the largest streaks in Couette flow.

Figure 4 shows the comparison between the absolute value of the main diagonal of $\mathbf{S}$, which corresponds to the power spectral density (PSD) of the three velocity components. We consider the response CSD of case $(n_\alpha, n_\beta) = (0, 1)$ using the statistics of the forcing obtained from the simulation without any correction ($\mathbf{P}_{DNS}$), the one considering the correction term ($\mathbf{P}_{DNS+c}$), and the one using the white-noise $\mathbf{P} = \gamma \mathrm{I}$ (with constant γ chosen so as to match the maximum PSD for this frequency). It can be seen that the shape of the main component (streamwise velocity u) can be fairly well reproduced by simply using $\mathbf{P} = \gamma \mathrm{I}$. Streaks are represented, with peak amplitudes distant of about 0.4 from the wall; this may be related to the higher shear near the walls, as shown in figure 1, leading to a stronger lift-up mechanism in that region. Considering white-noise forcing, we can see some discrepancies in the amplitudes and in some details of the shapes of the streamwise vortices (v and w components). Resolvent analysis (as formulated by McKeon & Sharma (2010)), assumes white-noise forcing, predicting thus streamwise vortices and streaks that are in reasonable agreement with the DNS, although with a mismatch in the relative amplitudes of u, v and w components; similar results were obtained for turbulent pipe flow by Abreu *et al.* (2019). This will be explored in more detail in § 4.1. For an accurate quantitative comparison, the statistics of the non-linear terms should be used; by doing that without the correction, the overall relative levels are closer to the one from the simulation, but the amplitudes are still off, especially at the peak of each component (which explains the errors seen in figure 3). When the correction is taken into account, the exact shapes are recovered for all components, without any rescaling.

The same process was carried out for case $(1, 0)$, and the results can be seen in figure 5. For this combination of wavenumbers, the flow is dominated by the spanwise velocity component, and the energy of the other velocity components are several orders of magnitude lower, as shown in figure 5. The dominance of w for the (1,0) mode was also observed by Smith *et al.* (2005); analysis of spectral density of turbulent channels also shows that structures with large spanwise extent are observed for w (del Álamo & Jiménez 2003). By considering white-noise statistics of the forcing, this dominance of spanwise velocity fluctuations could not be captured, and all components predicted by $\mathbf{R}\mathbf{R}^H$ have the same overall levels, leading to large errors for the (u, v) components. For the spanwise component, however, the position of the peak and the shape of $\mathbf{S}$ at the centre of the domain is roughly captured by the method, even though larger errors are found for regions closer to the wall. These facts altogether point out to an action of the non-linear terms in forcing mainly in the spanwise direction, with a more effective action closer to the wall (highlighted by the higher amplitude of the response around $y = 0.4, 1.6$). By including the uncorrected statistics of the forcing, $\mathbf{P}_{DNS}$, the problem of the relative amplitudes of the different components is solved; now the spanwise component dominates the response,

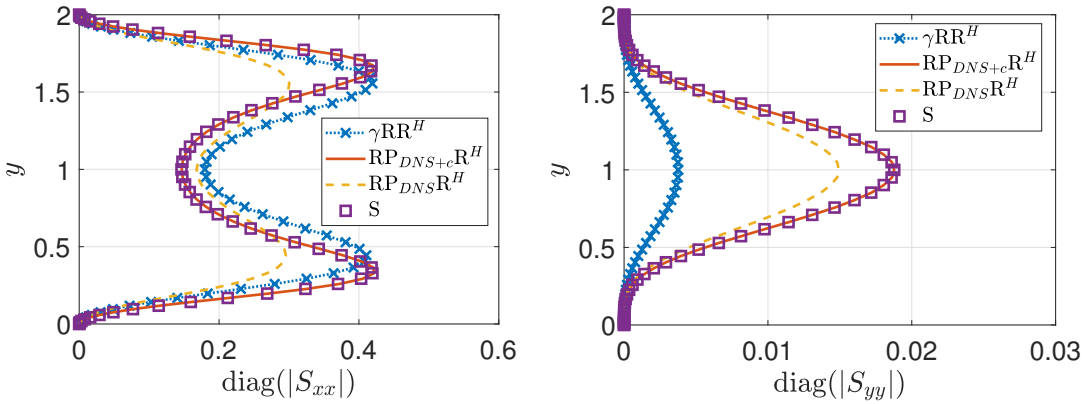

(a) Streamwise component

(b) Wall-normal component

(c) Spanwise component

Figure 4: **S** from simulation and from the recovery process using different **P** (white-noise, uncorrected and corrected) for case $(n_\alpha, n_\beta) = (0, 1)$. Prediction using white-noise **P** was scaled to match the maximum of **S** by the factor $\gamma = 1.029 \times 10^{-4}$.

and its shape resembles the one obtained directly from the simulation, even though a slight mismatch is found in the centre of the channel. This comparison is further improved by including the correction term in the statistics of the forcing; by using it, a perfect match between **S** computed from the simulation and the one from the forcing statistics is obtained, and the normalised error for this case is lower than 10^{-5}.

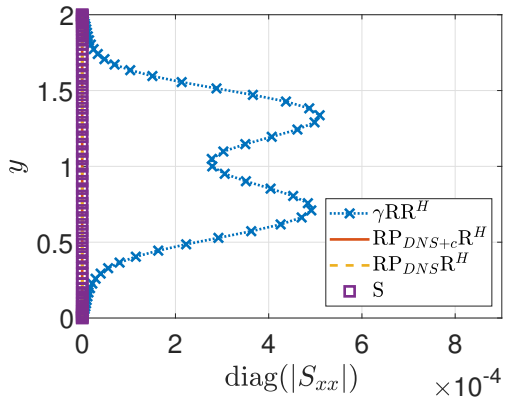

(a) Streamwise component

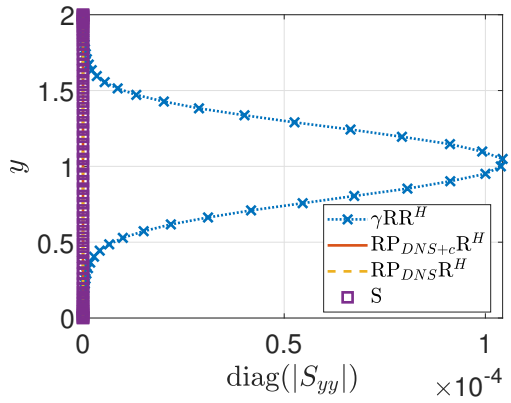

(b) Wall-normal component

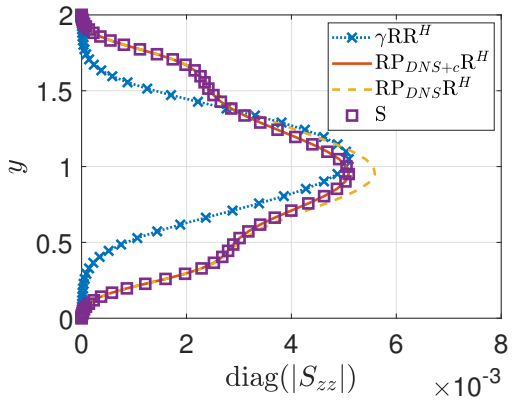

(c) Spanwise component

Figure 5: **S** from simulation and from the recovery process using different **P** (white-noise, uncorrected and corrected) for case $(n_\alpha, n_\beta) = (1, 0)$. Prediction using white-noise **P** was scaled to match the maximum of **S** by the factor $\gamma = 3.6295 \times 10^{-5}$.

4. Analysis of the forcing CSD

The previous analysis detailed the full response statistics recovery process, aiming at obtaining accurately the response statistics from the full statistics of the non-linear terms of the Navier-Stokes equations. However, the structure of the non-linear terms can be complex, and analysis of the full non-linear term can hardly lead to clear physical insight about the flow turbulent dynamics. For this reason, it would be interesting to simplify the forcing, with an evaluation of which components are mostly responsible for the energy of the response. This is performed in this section for wavenumbers $(n_\alpha, n_\beta) = (0, 1)$ and $(1, 0)$. The present analysis can uncover some of the physical mechanisms behind the action of the non-linear terms of the Navier-Stokes equations in the linearised operators, which can be useful in the design of turbulence models. Thus, in

this section we analyse the structure of the non-linear terms from the DNS, evaluating their relevant characteristics and performing simplifications whenever is possible. Inspired by this analysis, we inspect simple modelling approaches in Appendix B, pointing out how the simplest non-white $\mathbf{P}$ performs in this problem.

4.1. *Case* $(n_\alpha, n_\beta) = (0, 1)$

4.1.1. *Contribution of each component of the non-linear terms*

In this section we analyse more closely the structure of the non-linear terms for the case $(0, 1)$ for $\omega \to 0$ ($\omega = 0.0123$). Our objective here is to look closely at the forcing statistics in order to isolate the important parts for this simple case. The number of components of the non-linear terms, as defined in equation 3, makes an *ad hoc* modelling approach prohibitive; still, if only certain parts of the forcing are necessary to reproduce the statistics of the response, modelling can be considered an option. Specifically for the case $(n_\alpha, n_\beta) = (0, 1)$, the momentum equations 4b and 4c (v and w) decouple from the streamwise velocity, and these equations become also independent of the mean flow U. That allows us to rearrange the system in order to obtain separate equations for streamwise vortices (concentrated in the v, w components) and streaks (concentrated in the u component) as

$$\begin{aligned}\underbrace{\left[-\mathrm{i}\omega + \frac{1}{Re}\left(\beta^2 - \frac{\partial^2}{\partial y^2}\right)\right]}_{\mathbf{L}_{01}}\underbrace{\left(\beta^2 - \frac{\partial^2}{\partial y^2}\right)}_{\mathbf{B}_{01}} v &= \mathrm{i}\beta\left(-\mathrm{i}\beta f_y + \frac{\partial f_z}{\partial y}\right) \\ &= \left(\beta^2 - \frac{\partial^2}{\partial y^2}\right) f_y + \frac{\partial}{\partial y}\underbrace{\left(\frac{\partial f_y}{\partial y} + \mathrm{i}\beta f_z\right)}_{\text{zero response}} \\ &\Rightarrow \mathbf{L}_{01}\mathbf{B}_{01} v = \mathbf{B}_{01} f_y, \end{aligned} \tag{13}$$

$$\left[-\mathrm{i}\omega + \frac{1}{Re}\left(\beta^2 - \frac{\partial^2}{\partial y^2}\right)\right] u = f_x - v\frac{\partial U}{\partial y} \Rightarrow \mathbf{L}_{01} u = f_x - v\frac{\partial U}{\partial y}, \tag{14}$$

where the influence of the spanwise component of the forcing is already considered in equation 13, by considering that only the solenoidal part of the forcing leads to a response in velocity; inspection of the linear operators in the Orr-Sommerfeld-Squire formulation (Jovanovic & Bamieh 2005) confirms that hypothesis, which was also verified by Rosenberg & McKeon (2019) and Marsden & Chorin (1993). The spanwise component w can be obtained from v using the continuity equation. The linear optimal response of equation 13 for $\omega \to 0$ are streamwise vortices (as obtained from resolvent analysis), and these structures are independent of the mean flow chosen for the analysis, since the operators $\mathbf{L}_{01}$ and $\mathbf{B}_{01}$ do not depend on U. The effect of U is seen directly

in the equation of the streamwise velocity, via the $v\frac{\partial U}{\partial y}$ term, which is related directly with the lift-up effect: due to the presence of shear, these vortices will lead to the growth of streamwise velocity, which will assume the shape of streaks. One should note that there are two forcing terms in the right hand side of equation 14, which force directly the streaks; we would like to evaluate the influence of each one in the response. For that, we can rewrite the equation as a function of the expected value of u as

$$\mathbf{L}_{01}\mathcal{E}(uu^H)\mathbf{L}_{01}^H = \mathcal{E}\left[\left(f_x - v\frac{\partial U}{\partial y}\right)\left(f_x - v\frac{\partial U}{\partial y}\right)^H\right] \tag{15}$$

$$\begin{aligned}\mathbf{S}_{xx} = \mathbf{R}_{01}\Bigg[\mathbf{P}_{xx} + \left(\frac{\partial U}{\partial y}\right)\mathbf{S}_{yy}\left(\frac{\partial U}{\partial y}\right)^H \\ -\mathcal{E}(f_x v^H)\left(\frac{\partial U}{\partial y}\right)^H - \left(\frac{\partial U}{\partial y}\right)\mathcal{E}(v f_x^H)\Bigg]\mathbf{R}_{01}^H\end{aligned}, \tag{16}$$

where $\mathbf{R}_{01}$ is the resolvent operator associated with $\mathbf{L}_{01}$. The equation above shows that the statistics of the streamwise velocity can be educed from the statistics of the wall-normal velocity (which in turn can be obtained from the statistics of f_y), from the statistics of the streamwise component of the forcing f_x and from the cross-term statistics. Using the values obtained from the DNS, we can evaluate the influence of each term on the right hand side of equation 16: $\mathbf{P}_{xx}$ is related to the statistics of the streamwise component of the forcing; $(\frac{\partial U}{\partial y})\mathbf{S}_{yy}(\frac{\partial U}{\partial y})^H$ is related to statistics obtained using only the lift-up mechanism; the other components are the covariances between streamwise forcing and wall-normal velocity.

Figures 6(a-e) show the reconstruction of $\mathbf{S}_{xx}$ using each term of equation 16 (just the real part is shown). As expected, the reconstruction using all terms reproduces the results from the DNS; on the other hand, if we take only the term related to the lift-up mechanism, the shapes of $\mathbf{S}_{xx}$ differ, especially considering the position of the peaks. The same happens when we use only the term related to the statistics of the forcing in the streamwise direction, or when we use only the cross-terms (which have a negative contribution of the sum). Still, the sum of all these quantities generates a combination of constructive-destructive influence on $\mathbf{S}_{xx}$, leading to the correct shape and amplitude, when all terms are considered. This can be better understood by looking at power spectral density (which is the main diagonal of $\mathbf{S}$) using each term, compared to DNS results. This is shown in figure 6(f), where we can see that, even though the amplitudes of each component are high, the final result considering all terms is rather small, and the contribution of the cross-term seem to be responsible for this overall reduction. The negative effect of the cross-term thus represents a destructive interference between the lift-up mechanism and the direct excitation of streaks by the streamwise forcing component. This effect cannot be appropriately modelled when the forcing is considered as white noise, as seen in § 3.2.

This analysis highlights that consideration of isolated mechanisms (such as lift-up only or streamwise forcing only) may lead to quantitative errors in the prediction of flow responses. Similar results were obtained by Freund (2003); Bodony & Lele (2008) and Cabana *et al.* (2008) in studies of sound generation by a sheared flow, using Lighthill's acoustic analogy. The cited works showed that when source terms, analogous to the forcing CSD $\mathbf{P}$ considered here, are decomposed into subterms, an analysis of the isolated contribution of each one may be problematic, as destructive interference between components may lead to a summed radiation which is lower than the individual contributions. In the context of wall-bounded flows, Rosenberg & McKeon (2019) also noticed a similar destructive interference phenomenon for the terms composing the $\langle uv \rangle$ Reynolds stress for an exact coherent state in channel flow. The authors pointed out that modes forced by different mechanisms may have similar absolute value but opposite phase, leading to a smaller amplitude for the quantity, similar to the behaviour observed in figure 6(f). The present analysis shows that a similar effect occurs in the analysis of the streamwise velocity covariance in turbulent Couette flow.

4.1.2. *Contribution of each component of the non-linear terms*

From the preceding analysis we can understand that all components (lift-up related and streamwise forcing) are important to obtain good predictions of $\mathbf{S}$. Nevertheless, some simplification can still be performed on the forcing terms by rewriting them as the sum of the non-linear terms of the Navier-Stokes equations. Overall, these terms can be written as

$$\tilde{f}_i|_{\omega\neq 0} = -\tilde{u}_j \frac{\partial \tilde{u}_i}{\partial x_j} \tag{17}$$

or, in vector form

$$\tilde{\mathbf{f}}|_{\omega\neq 0} = \begin{pmatrix} \tilde{f}_x|_{\omega\neq 0} \\ \tilde{f}_y|_{\omega\neq 0} \\ \tilde{f}_z|_{\omega\neq 0} \end{pmatrix} = -\tilde{u} \begin{pmatrix} \frac{\partial \tilde{u}}{\partial x} \\ \frac{\partial \tilde{v}}{\partial x} \\ \frac{\partial \tilde{w}}{\partial x} \end{pmatrix} - \tilde{v} \begin{pmatrix} \frac{\partial \tilde{u}}{\partial y} \\ \frac{\partial \tilde{v}}{\partial y} \\ \frac{\partial \tilde{w}}{\partial y} \end{pmatrix} - \tilde{w} \begin{pmatrix} \frac{\partial \tilde{u}}{\partial z} \\ \frac{\partial \tilde{v}}{\partial z} \\ \frac{\partial \tilde{w}}{\partial z} \end{pmatrix} = \tilde{\mathbf{f}}_u + \tilde{\mathbf{f}}_v + \tilde{\mathbf{f}}_w. \tag{18}$$

Individual terms are evaluated in physical space and transformed to frequency-wavenumber space afterwards. Writing the forcing this way allows us to decompose $\mathbf{P}$ into 9 components, related to each of the 3 forcing terms in equation 18 and extract the relevant parts of this term. Due to the low number of forcing components to evaluate, we chose to remove some of them by trial and error, in order to evaluate the influence of those in the statistics of the response. A first analysis shows that $\tilde{\mathbf{f}}_u$ does not play a significant role in this case, as predictions of the shapes of $\mathbf{S}$ disregarding this term did not lead to any considerable mismatch. The terms $\tilde{v}\frac{\partial \tilde{v}}{\partial y}$ and $\tilde{v}\frac{\partial \tilde{w}}{\partial y}$ are also less relevant for this case. This reduces the forcing to

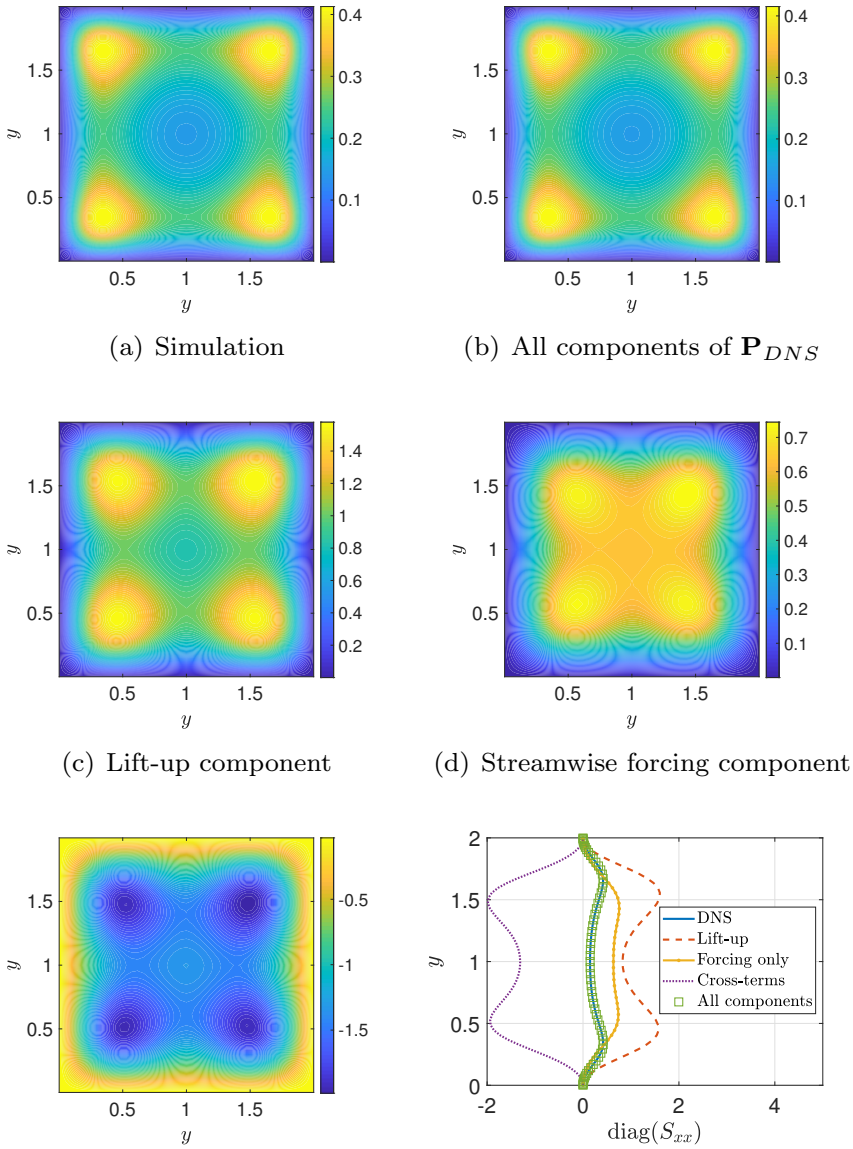

(a) Simulation (b) All components of $\mathbf{P}_{DNS}$

(c) Lift-up component (d) Streamwise forcing component

(e) Cross-terms (f) Sum of the contributions

Figure 6: Real part of streamwise component of **S** from simulation (a) and the prediction using different forcing term (b-e). Contribution of each term in the reconstruction (f).

$$\tilde{\mathbf{f}}_{red}|_{\omega\neq 0} = -\tilde{v}\begin{pmatrix}\frac{\partial\tilde{u}}{\partial y}\\ 0\\ 0\end{pmatrix} - \tilde{w}\begin{pmatrix}\frac{\partial\tilde{u}}{\partial z}\\ \frac{\partial\tilde{v}}{\partial z}\\ \frac{\partial\tilde{w}}{\partial z}\end{pmatrix} = \tilde{\mathbf{f}}_{v_x} + \tilde{\mathbf{f}}_{w}. \tag{19}$$

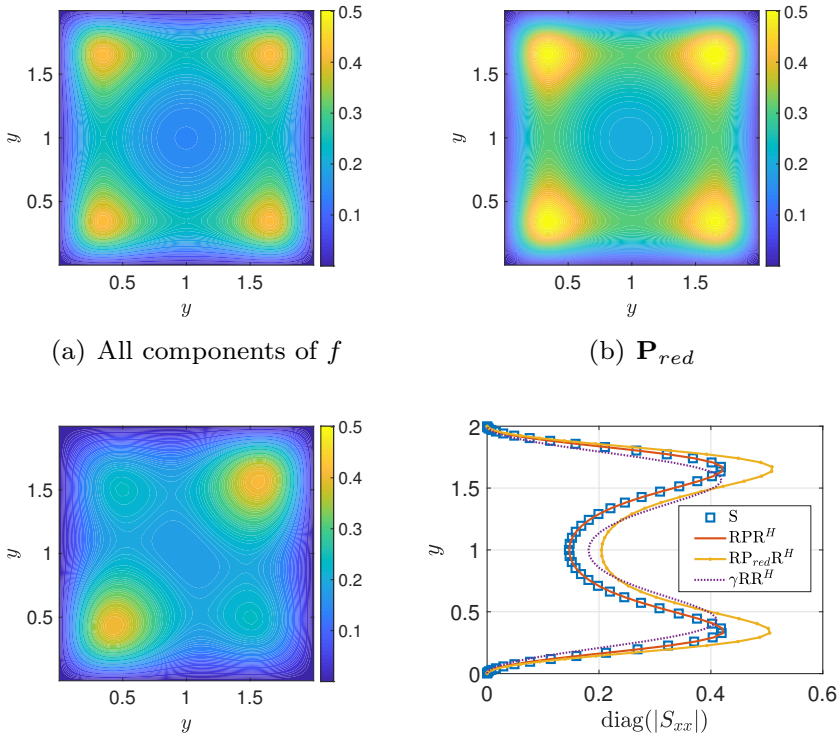

(a) All components of f (b) $\mathbf{P}_{red}$

(c) White-noise $\mathbf{P}$ (d) Main diagonal of $\mathbf{S}$

Figure 7: Streamwise component of $\mathbf{S}$ from the reconstruction using the whole forcing (a), the reduced order forcing (b), statistical white forcing (c) and the absolute value of the diagonal of each one compared with the one from the simulation (d).

This is the maximum simplification that the covariance of the forcing can suffer in order to recover the covariance of the response without introduction of significant error in its shape. A final evaluation of the influence of the reduction is performed in section 4.1.3, showing that the most energetic structures of the flow for these reduced covariances are virtually unchanged.

The cross-spectral density $\mathbf{S}$ recovered using the total forcing, the reduced forcing and the white-noise forcing can be seen in figure 7. From figures 7(a-c), it is clear that the reduction of the forcing to the expression 19 leads to the correct amplitude distribution of the streamwise velocity CSD, with better agreement than consideration of white-noise forcing; in particular, the coherence between the two peaks in amplitude, which can be seen by the nearly identical values for (y, y) and $(y, -y)$, is recovered from $\mathbf{P}_{red}$. Still, by retaining only the terms in eq. 19, a mismatch starts to appear in the amplitudes of the reconstruction, as shown in figure 7(d).

4.1.3. *Low rank of forcing*

We now consider the most energetic structures in the flow, extracted using Spectral Proper Orthogonal Decomposition (SPOD) for this combination of frequency-wavenumber. In particular, we evaluate if forcings and responses have low rank, which may simplify the modelling. Figure 8(a) shows the eigenvalues of the SPOD of the full covariance of the forcing, the reduced one (both considering the correction in eq. 25), and the covariance of the response. SPOD here amounts simply to an eigendecomposition of the mentioned cross-spectral densities, which are Hermitian by construction. In figure 8(a) we can see that there is a clear separation between the first and the following modes for these matrices; therefore, the first SPOD mode would be sufficient to represent the forcing and response. Also, the energies of the covariance of the reduced forcing $\mathbf{P}_{red}$ are close to the ones of the full $\mathbf{P}$, which highlights the similarities between the two matrices. The comparison between the leading SPOD mode of the response (denoted as follows as SPOD-q) and the reconstruction using $\mathbf{q} = \mathbf{R}\mathbf{f}_{SPOD}$ (where $\mathbf{f}_{SPOD}$ is the first SPOD mode of the corrected forcing, both full and reduced) is shown in figure 8(b). These plots show clearly that the leading SPOD mode of both $\mathbf{P}$ and $\mathbf{P}_{red}$ lead to close agreement with the first SPOD mode of $\mathbf{S}$, which confirms that the terms in equation 19 are, indeed, the dominant ones in this problem. Figure 8(b) also show that the first resolvent mode, computed under the hypothesis of white-noise forcing, does not match the SPOD mode from the simulation, showing that the statistics of the non-linear terms are important to match exactly the shapes of the most energetic structures of the flow (Zare *et al.* 2017; Towne *et al.* 2020). The main shapes are nonetheless retrieved in the leading response mode of resolvent analysis, with v and w forming a streamwise vortex, as seen for instance in the amplitude distribution of w, with two lobes in phase opposition, and an amplified streak in u. There is a mismatch in the relative amplitudes of the streamwise vortex and the streak, which is corrected when the forcing statistics are considered.

We can also evaluate the most energetic structure of the non-linear terms; considering that we are interested in their physical shapes, we calculated the SPOD of $\mathbf{P}$ without the correction term. The first SPOD mode of the forcings for the considered frequency is shown in figure 9. Even though the leading mode of the full forcing has an intricate structure (especially due to the presence of an extra oscillation in the centre of the domain in the wall-normal velocity), the first SPOD mode of the reduced forcing, from eq. 19 is clear, at least considering the spanwise and wall-normal components, with the shape of a streamwise vortex (also shown in figure 9(b), where the mode was reconstructed using the wavenumbers for this case). This connects directly with the conclusions drawn previously: the streamwise vortices of the response are excited by streamwise solenoidal forcing from the non-linear terms; these vortices, in turn, feed the lift-up effect such that streaks appear in the velocity field. Considering that we are dealing with the non-linear term of the Navier-Stokes equations, this result

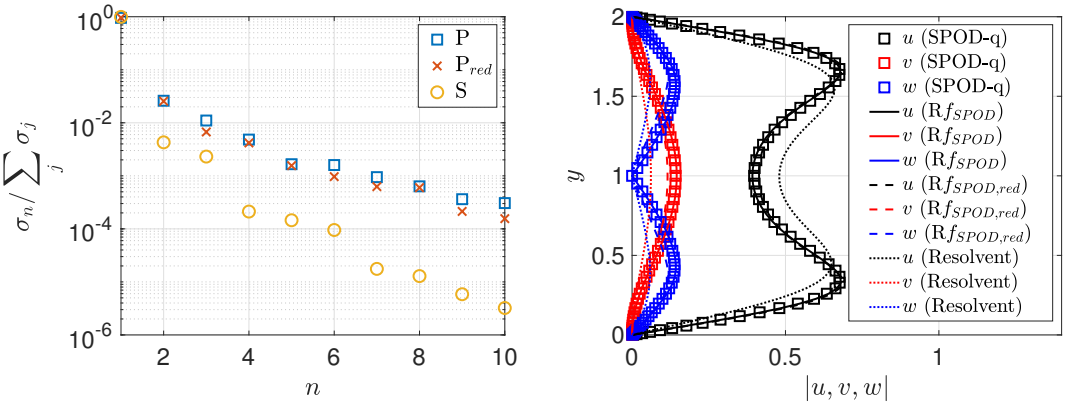

(a) SPOD eigenvalues (b) Leading SPOD mode and reconstructions

Figure 8: SPOD eigenvalues for **S** and the different **P** used here (a) and the shapes of the leading SPOD mode of the response (SPOD-q) compared with the reconstruction using the leading SPOD mode of the forcing and the first response mode from resolvent (b).

may be seen as surprising. The non-linear forcing term gathers the contribution of all triadic interactions that affect the considered frequency and wavenumber, being fed by a myriad of combinations of frequencies and wavenumbers. Still, the dominant part of these non-linear combinations in the y and z directions (related to the $\tilde{w}\partial\tilde{v}/\partial z$ and $\tilde{w}\partial\tilde{w}/\partial z$ terms) will generate a streamwise vortex in the forcing. However, the streamwise vortical forcing alone is not sufficient in order to match the response; a distribution of streamwise forcing, related to $\tilde{v}\partial\tilde{u}/\partial y$ and $\tilde{w}\partial\tilde{u}/\partial z$, is essential to recover the correct response. Finally, the appearance of w in all forcing directions (in equation 19) also shows that the spanwise velocity fluctuations greatly affects the forcing term for the mode $(0, 1)$. Therefore, any combination of triadically interacting Fourier modes dominated by w is likely to have a contribution to this forcing term and to the dynamics of the $(0, 1)$ wavenumber.

One can also think of the most energetic structure of the forcing in light of the lift-up effect. Figure 10 shows the comparison between velocity components from the first SPOD mode and the linear optimal response mode from resolvent analysis, now rescaled to have matching wall-normal components. From this plot, it is clear that the shapes of the vortices from resolvent analysis and SPOD are in close agreement. Still, by performing such scaling, the streak associated with the resolvent response has a much larger amplitude than the one from SPOD. This can be connected to the phenomenon seen in Figure 9(b): considering that there are large portions of negative streamwise forcing at positions where the vertical forcing would induce a positive streak via the lift-up effect, this component of the non non-linear terms acts as a destructive interference in its peak positions, substantially decreasing the amplitude of the

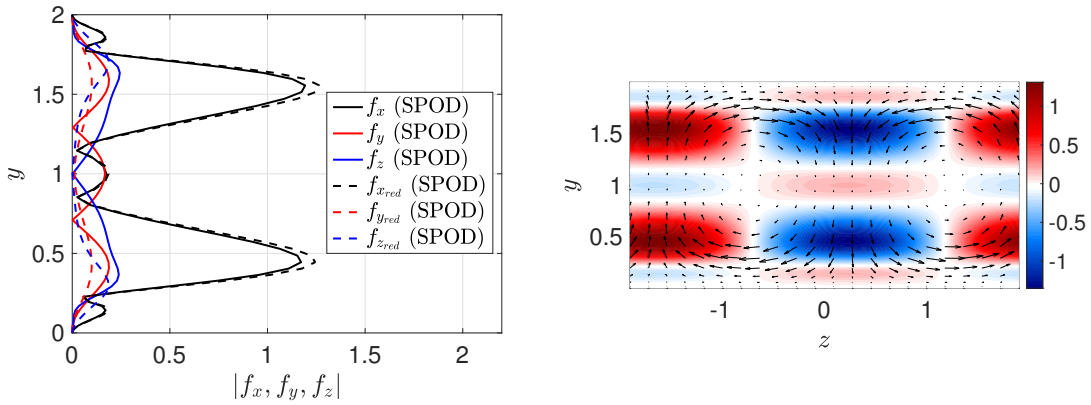

(a) Absolute value of first SPOD mode of the forcings (b) Reduced forcing in the physical space

Figure 9: Absolute value of first SPOD mode of the full and reduced forcings (a) and the shape of the reduced forcing in the physical space. Colours: streamwise forcing; arrows: wall-normal and spanwise forcings.

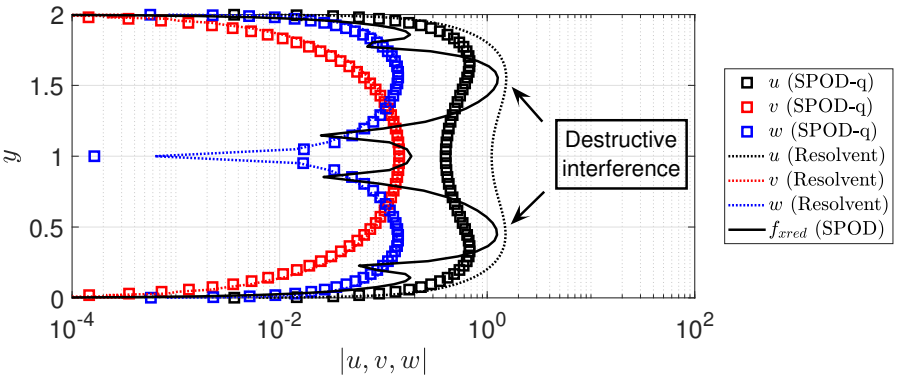

Figure 10: Sketch of the action of the non-linear terms on the optimal response of mode $(0, 1)$. All quantities are defined as in figures 8(b) and 9(a), and the arrows point to the regions of the flow where the destructive interference/cancellation effect is more pronounced. Log scale is used to provide a better visualisation of the agreement between resolvent and SPOD vortices, and to highlight the amplitude mismatch between the streaks.

streaks, and slightly changing its overall wall-normal shape. Therefore, the effect of the forcing in this case is mostly to cancel the streak generated by the linear mechanism, decreasing the streak-to-vortex amplitude ratio, thus leading to the structure found in the SPOD. This is shown schematically in figure 10.

4.2. *Case* $(n_\alpha, n_\beta) = (1, 0)$

4.2.1. *Contribution of each component of the non-linear terms*

We now analyse the case $(1, 0)$, also taken at the limit $\omega \to 0$ ($\omega = 0.0123$, as in the previous section). Analysis of the energy related to each velocity component for this case points to a dominance of w fluctuations for the present mode. Since the dynamics of w is uncoupled from the rest (by inspection of equation 4c), it is sufficient to analyse the non-linear terms related to f_z to recover the correct statistics of the velocity, which will also be dominated by the spanwise component, as observed in the DNS data.

The z component non-linear terms can be written as

$$\tilde{f}_z|_{\omega\neq 0} = \underbrace{-\tilde{u}\frac{\partial \tilde{w}}{\partial x}}_{\tilde{f}_u} \underbrace{-\tilde{v}\frac{\partial \tilde{w}}{\partial y}}_{\tilde{f}_v} \underbrace{-\tilde{w}\frac{\partial \tilde{w}}{\partial z}}_{\tilde{f}_w}, \tag{20}$$

which is already simpler than the previous case, since the full forcing term only has the contribution of only three terms. We can perform the same analysis as in the previous case and try to remove some of the terms in order to check the impact of each one in the statistics of the response. The reductions that led to similar shapes for the statistics of the response are the combinations $\tilde{f}_u + \tilde{f}_v$ (nearly perfect agreement) and $\tilde{f}_u$ (mismatch in amplitude). The reconstructions of $\mathbf{S}$ using each of these combination of terms is shown in figure 11.

As expected, the reconstruction using all components of the forcing term recovers very accurately $\mathbf{S}$ from the simulation, as well as by using just the terms $\tilde{f}_u$ and $\tilde{f}_v$. A further reduction (using just $\tilde{f}_u$) also gives overall correct shapes, but an amplitude mismatch appears for the computed $\mathbf{S}$, as shown in figure 11(f). No other simplification led to accurate recovery of $\mathbf{S}$. These plots also highlight the need of using the statistics of the forcing for the prediction of the response for this mode: figures 11(e,f) show that consideration of white-noise statistics for the forcing leads to inaccurate shapes for the statistics of the response, even though the peak is roughly captured.

4.2.2. *Low rank of forcing and response*

Taking SPOD modes of $\mathbf{S}$ and of the corrected $\mathbf{P}$ (both full and reduced), we obtain the gains shown in figure 12(a). It is clear that, for the present frequency, these matrices are also low-rank: the first SPOD mode is at least one order of magnitude higher than the other ones, pointing out that using only the first SPOD mode is sufficient to represent the forcing and the response. For a reconstruction using the first SPOD mode of the forcings, we obtain modes very close to the first SPOD mode of the response for all cases; even the more drastic reduction, considering only $\tilde{f}_u$, leads to a close agreement with the response statistics for most positions, with a slight mismatch above the centerline. As expected, given the differences between the prediction using the white-noise $\mathbf{P}$ and the covariance of the response from the simulation, the first resolvent mode

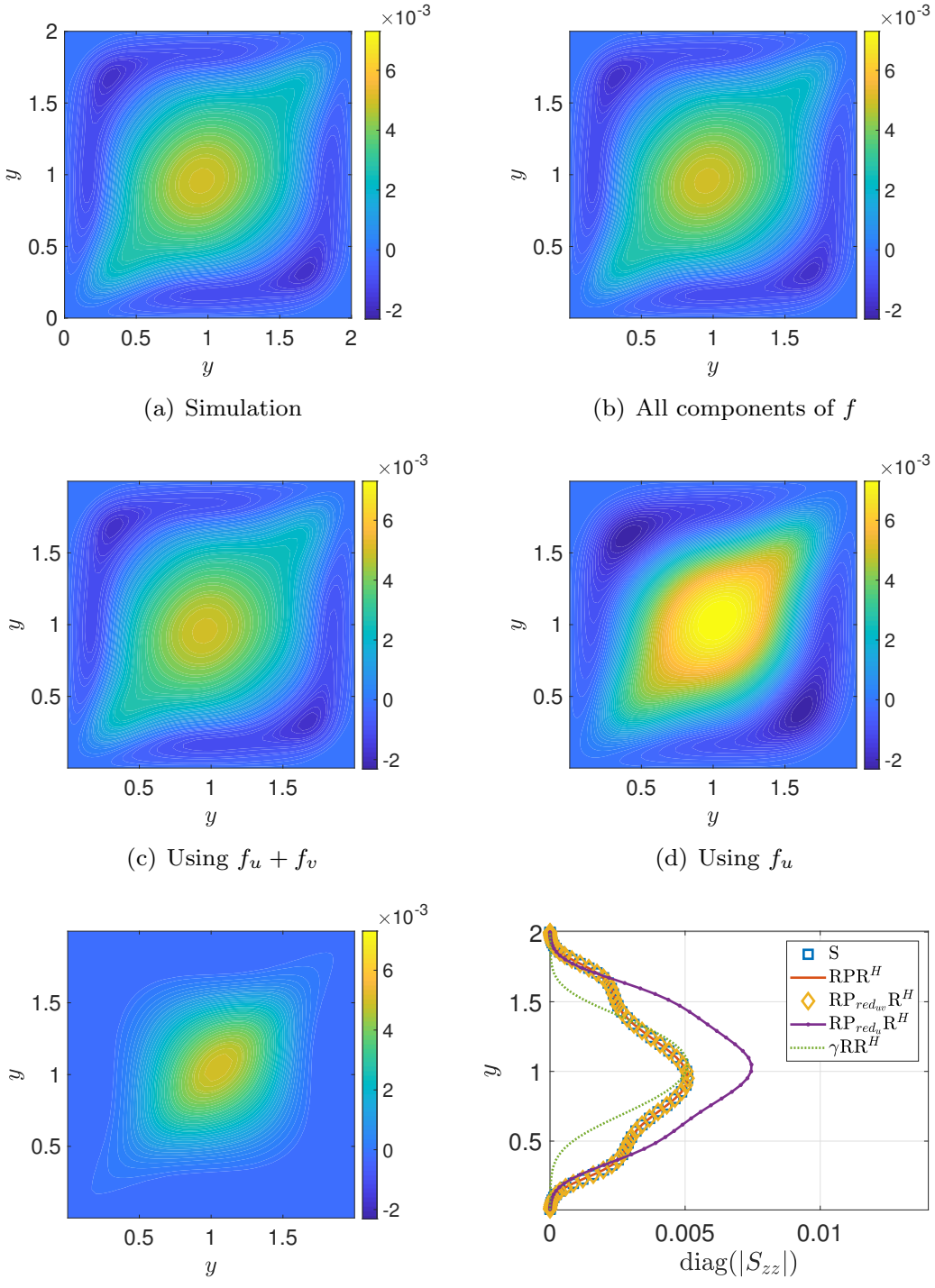

Figure 11: Streamwise component of **S** from the velocity field (a), from the reconstruction using the whole forcing (b), the reduced order forcing with $\tilde{f}_u + \tilde{f}_v$ (c), the reduced order forcing with $\tilde{f}_u$ (d), statistical white forcing (e) and the absolute value of the diagonal of each one compared with the one from the simulation (f).

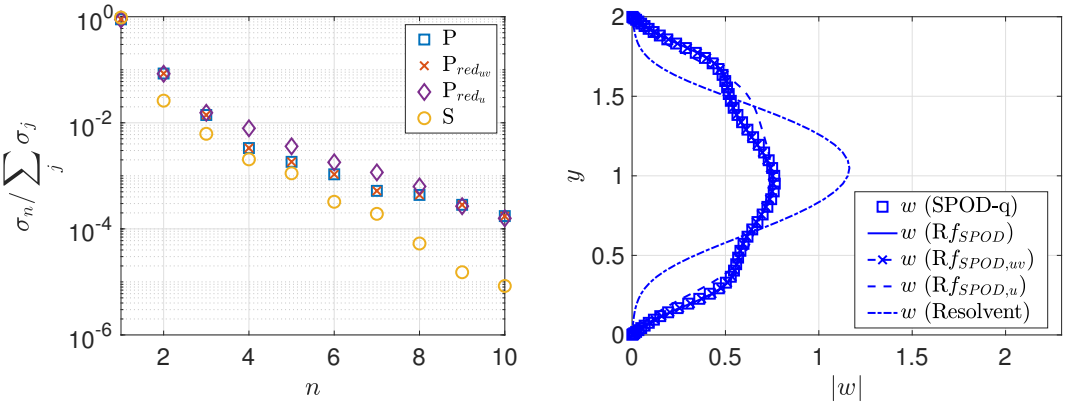

(a) Gains (b) SPOD modes and reconstructions

Figure 12: Energies from SPOD for **S** and the different **P** used here (a) and the shapes of the SPOD mode of the response compared with the reconstruction using the first SPOD mode of the forcing (b).

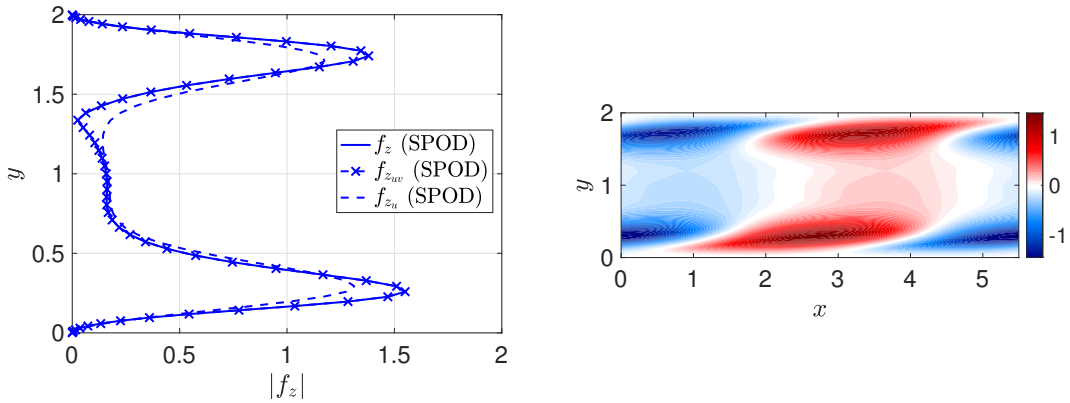

(a) Absolute value of first SPOD mode of the forcings (b) Reduced forcing f_u in the physical space

Figure 13: Absolute value of first SPOD mode of the full and reduced forcings (a) and the shape of the reduced forcing in the physical space. Colours: spanwise forcing.

does not capture the correct shape of the most energetic structure in the flow, especially close to the wall.

Finally, we can also look at the shapes of the leading SPOD mode of the forcing for this case. Figure 13 shows that the reduction of the forcing to $\tilde{f}_u$ only does not lead to any substantial changes in the optimal forcing from SPOD; the $\tilde{f}_v$ component adjusts the shape of forcing structure in some specific regions, without a major role in the bulk shape. In figure 13(b) we can see the reduced

forcing in the physical space. The peaks, for this case, are concentrated in regions close to the wall, which explains why the difference between resolvent and SPOD modes is more evident in these regions; since f_z is higher in that region, the first SPOD mode also has higher amplitudes closer to the wall.

From these results, we can see that the case $(1, 0)$ is mostly dependent on the term $\tilde{f}_z$. Since the forcing is mainly dependent on $\tilde{u}\partial\tilde{w}/\partial x$, as shown in figure 13(a), it is expected that the triadic interactions composed by terms with wavenumbers pairs with high streamwise velocity amplitudes will affect the non-linear term more substantially. This is confirmed in the next section.

5. Relation with the self-sustaining process

This work was based on the minimal flow unit for Couette flow, the minimal computational box in which turbulence can be sustained. This case was developed by Hamilton *et al.* (1995), who also proposed a self-sustaining process for the turbulence in this simple shear flow. Considering that the structures present in this flow are ubiquitous to all shear flows, the proposed mechanism has also been extended to several other cases (see Jiménez & Pinelli (1999); Schoppa & Hussain (2002), for example). This can be summarised as: (1) streaks are produced as a result of the lift-up effect (Ellingsen & Palm 1975); (2) the growth of the streaks leads to an instability in the flow, which triggers the breakdown of these structures; (3) streamwise vortices are regenerated via a non-linear mechanism, thus leading to a regeneration of the streaks. With this process in mind, we can explore the possible reasons why only some of the terms from the non-linear forcing are relevant for capturing the overall low-frequency dynamics of this flow, as shown in section 4. First, it should be expected that velocity fluctuations $\tilde{v}$ would play a role in this case, considering that the lift-up effect is the dominant phenomenon in this sheared flow. It is thus relevant to examine in detail how vertical velocity fluctuations $\tilde{v}$, associated with streamwise vortices in the (0,1) wavenumber, are forced by non-linear terms. Two possible candidates for a consistent triadic interaction would be wavenumbers (1,0) and (1,1). As shown by Hamilton *et al.* (1995), mode (1,0) is one of the most energetic ones in this flow, and the triadic interaction between this spanwise velocity-dominated mode, and mode (1,1) (which shows no dominant velocity component) would be expected to be one of the main mechanism of energy transfer to mode (0,1) – thus, $\tilde{w}^{(1,0)}\partial\tilde{u}_i^{(1,1)}/\partial z$ should be a dominant part of the forcing associated with $\tilde{v}^{(0,1)}$, since this is the relevant forcing component in the y direction, as examined in § 4.1.

The above arguments suggests how an interaction between (1,0) and (1,1) modes would force the (0,1) mode. A similar argument can be formulated to explore how triadic interactions give rise to the term $\tilde{u}\partial\tilde{w}/\partial x$ in mode (1,0), shown to be dominant in § 4.2: since the streamwise velocity component of mode (0,1) has a high amplitude, the triadic interaction between $\tilde{u}$ from this mode and $\partial\tilde{w}/\partial z$ from mode (1,1) should affect the temporal evolution of mode (1,0).

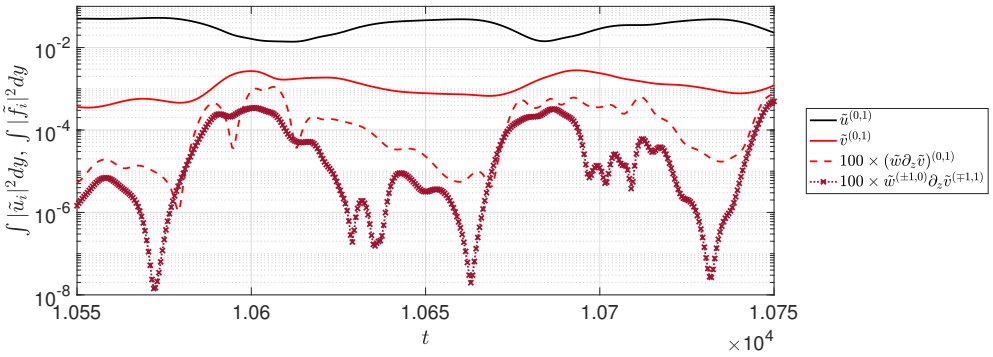

(a) Mode (0,1)

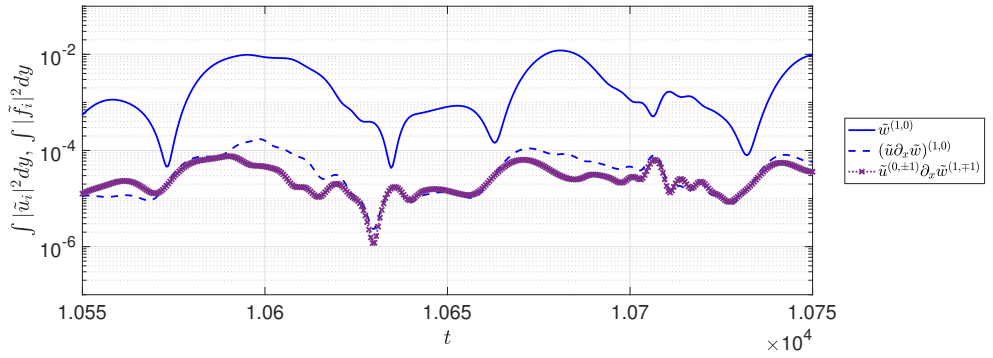

(b) Mode (1,0)

Figure 14: Integrated energy as a function of time of streamwise velocity of modes (0,1) and (0,1), and relevant non-linear term for each combination of wavenumbers, as discussed in the text. Triadic interactions between the most energetic modes leading to the non-linear terms for each case are also shown. Interaction between modes (1,0) and (1,1) considers the contribution of wavenumber combinations (-1,0)/(1,1) and (1,0)/(-1,1), and equivalently for modes (0,1) and (1,1).

Figure 14 shows some of the relevant quantities for two cycles of the present simulation. The process of generation and breakdown of streaks can be tracked by looking at the streamwise component of the velocity for mode (0,1) in figure 14(a). Streak breakdown (intermittent decay of the amplitude of $\tilde{u}^{(0,1)}$) is closely associated with an increase of the amplitudes of $\tilde{v}$. Considering that the evolution of the streamwise velocity does not affect the evolution of the wall-normal component except via non-linear terms (as shown in equation 13), this growth in $\tilde{v}$ should be related to the equivalent non-linear forcing in the y direction. Figure 14(a) shows that the most relevant component of this forcing, $\tilde{w}\partial\tilde{v}/\partial z$ (as shown in § 4.1), follows the evolution of the wall-normal velocity, with matching regions of growth/decay. Since this non-linear forcing can be explicitly written as the sum of the triadic interaction between modes

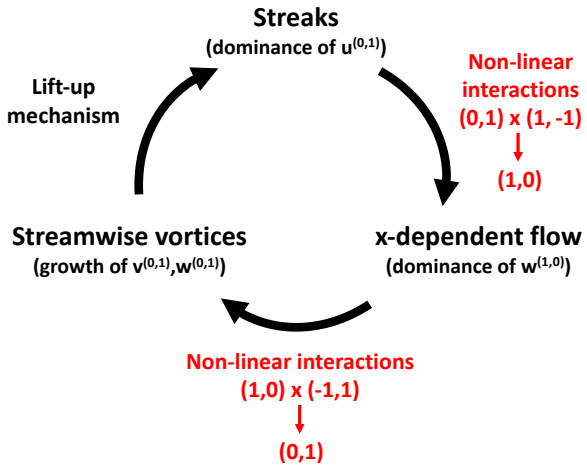

Figure 15: Self-sustaining process in turbulence as proposed by Hamilton *et al.* (1995). The vortex regeneration mechanism obtained from non-linear interactions analysed in the present study is shown in red. The non-linear interaction from "streaks" and "x-dependent flow" is associated with the saturation of streaks.

with summed wavenumbers resulting in mode (0,1), it is expected that the interaction between energetic modes should contribute greatly to this term. In fact, the non-linear term computed from the interaction between modes (1,0) and (1,1) (also shown in figure 14(a)) seems to follow the same growth/decay trend with similar absolute value for high-amplitude periods, pointing to a connection between the evolution of the spanwise velocity of mode (1,0) and the regeneration of vortices.

Similarly, the energy of mode $(1,0)$ is basically due to $\tilde{w}$. It is shown in figure 14(b), where the dominant part of the forcing term for mode (1,0) and the dominant triadic interation between modes (0,1) and (1,1) are also depicted. It is clear that the evolution of the spanwise velocity is closely related to the evolution of the forcing term – growth and decay regions of the velocity follow the same regions of the forcing with a time delay. For this mode, the forcing is dominated by the non-linear term associated with the most amplified streak interacting with mode (1,1). Therefore, even though the linearised Navier-Stokes equation for $\tilde{w}^{(1,0)}$ does not depend on the other velocity components with the same wavenumber (as mentioned in section § 4.2), its evolution is still determined by the evolution of the streaks via non-linear interactions. Considering that no clear forcing reduction was found for mode (1,1), the role of this mode is highlighted here as an "inter-wavenumber energy transfering" mode in this dynamics, connecting streaks to the spanwise velocity mode. We show that this is a crucial element in the vortex regeneration process.

In summary, energy flows from the streak (in $\tilde{u}^{(0,1)}$) to the spanwise velocity mode via triadic interactions with mode (1,1), which leads to an increase of $\tilde{w}^{(1,0)}$. This growth, in turn, leads to an increase of the non-linear forcing related to the vortices of mode (0,1), regenerating these structures. Finally, these will regenerate the streaks in the flow via the lift-up effect. This vortex regeneration mechanism is summarised in figure 15, as an addendum to the diagram proposed by Hamilton *et al.* (1995). As a consequence of that, the dynamics of the spanwise velocity for mode $(1, 0)$ (followed closely by its main forcing component) opposes the trend of the streamwise velocity of mode $(0, 1)$, which agrees with the analysis of streak breakdown for Couette flow performed by Schoppa & Hussain (1999). The authors show that the streak instability is triggered by streamwise varying, low-amplitude spanwise velocity disturbances; therefore, it is expected that an increase in the w component of the velocity will lead to the breakdown of the streaks. Hamilton *et al.* (1995) observed that the amplitudes of this component can reach the same order of magnitude of the streamwise component during streak breakdown, highlighting the importance of the underlying dynamics followed by $\tilde{w}^{(1,0)}$ in this flow. The relevance of this mode was further detailed in the present analysis, where its role in the non-linear dynamics of the flow is also explored. The analysis in section 4.1 has shown that this component is essential for the recovery of the velocity statistics of streaks; the simplified forcing of eq. 19 has its streamwise vortical component, f_w, strongly related to fluctuations in w. Therefore, in order to recover the energy of mode $(0, 1)$ (thus leading to streak regeneration), higher amplitudes of spanwise velocity should be present in the flow.

6. Conclusions

Using a direct numerical simulation of a minimal flow unit, taken for turbulent Couette flow at $Re = 400$, we carried out an analysis of the non-linear terms of the Navier-Stokes equations expanded around the mean turbulent field, built as the product of velocity fluctuations in the physical domain. It is shown that, even though resolvent response modes coming from linear analysis correspond to SPOD modes if the non-linear terms are uncorrelated, the statistics of these terms actually play a substantial role in some cases, changing the shape of the resulting energetic modes. Therefore, a proper consideration of these statistics is necessary for high-fidelity response prediction, leading to considerable improvements over the white-noise assumption often used. By detailing the process of recovering the frequency-domain statistics of the velocity from the statistics of the non-linear terms (treated as a forcing term, in a resolvent formulation), we managed to understand the influence of the windowing in the equations, which gives rise to new terms that must be included in the formulation, as proposed by Martini *et al.* (2019); in the present work, we further show the validity of this result by applying the methodology for the analysis of a turbulent flow. Most of the comparisons between SPOD and resolvent modes in the literature do not consider, to the best of our knowledge, the error due to windowing. For lower frequencies, this may lead to unexpected errors that

may deteriorate the comparisons. In order to correctly evaluate the validity of the models using linear analysis, a correction term should be considered as an additional forcing (as done in the present work), or as a correction of the statistics of the velocity. For the present analysis, this error mainly affects low frequencies/wavenumbers. When the appropriate correction is included, relative errors of about 10^{-5} are obtained, which ensures the accuracy of the obtained cross-spectral densities of forcing and response for this flow.

Considering that the CSDs of forcing ($\mathbf{P}$) and response ($\mathbf{S}$) are accurately related to each other by the resolvent operator, we further analysed the linearised Navier-Stokes equations in order to evaluate which parts of the forcing were relevant for the prediction of the statistics of the velocity. This was done for the two most energetic cases at low frequencies: the case $(n_\alpha, n_\beta) = (0, 1)$ (streaks), and $(n_\alpha, n_\beta) = (1, 0)$ (spanwise velocity modes). These analyses were performed for $\omega \to 0$, as spectra for the two wavenumbers have highest levels for the lowest frequencies, a consequence of the zero phase speed of dominant modes in Couette flow with walls moving in opposite directions. The first mode, $(0, 1)$, is characterised by the appearance of streaks and streamwise vortices. We have shown that using spatial white-noise as statistics of the forcing leads to a partial agreement between the prediciton of the covariance of the response using the resolvent operator and the one obtained from the simulation; even though streamwise vortices and streaks are obtained from white-noise forcing, there is a mismatch in their relative amplitudes. The forcing is shown to act with a destructive interference between direct forcing of streaks by streamwise forcing and the lift-up mechanism, where the streamwise vortical part of the forcing leads to streamwise vortices and streaks. This behaviour is similar to the one observed by Rosenberg & McKeon (2019) for the $\langle u, v \rangle$ statistics in the case of an exact coherent state in channel flows. Simplification of non-linear terms is also possible, with four of them (among nine possible ones) leading to the bulk of the response statistics; of particular relevance is the contribution of spanwise velocity in forcing, as it appears in three of the four dominant terms.

The same process was performed for the wavenumber $(1, 0)$. The equations for this case decouple for the spanwise velocity. As this component is the most energetic one for this case, only the spanwise forcing would be needed to recover most of the covariance matrix of the response. By applying the same process as the previous case, we manage to reduce the forcing to only one term, $\tilde{u}\partial\tilde{w}/\partial x$. Simplification of the forcing as white noise again led to a mismatch in the predicted flow responses; here, the amplitude distribution of the forcing, which is stronger closer to the walls, is a salient feature, leading to the observed flow response. Even though no significant forcing reduction was found for mode (1,1), a connection with this oblique wave mode was also made in the self-sustaining process framework, showing that the interaction between the streaks and the (1,1) wavenumber mode dominates the excitation of mode (1,0). By analysing the non-linear terms from the DNS, we managed to isolate dominant terms and interactions in the excitation of each mode, clarifying some of the relevant steps

of the vortex regeneration process. In summary, energy is transferred from mode (0,1) (streaks) into (1,0) (spanwise velocity) through the oblique wave mode (1,1). This is followed by a second interaction, where energy is transferred from the (1,0) mode (and the oblique (1,1)) back into the (0,1) mode through the breakup of of the x-dependent motions.

Even though only two wavenumbers were analysed in this work, the conclusions presented herein lead to a better understanding of the turbulence dynamics in wall-bounded flows. Instead of modelling the effects of the non-linearities, we show the structure of the non-linear terms explicitly, pointing out that these can be simpler than the general understanding. Moreover, the cases studied are connected to the self-sustained process in turbulence, which is considered to be one of the building blocks of the turbulent flows; knowing more about the action of the non-linearities in such case affects the understanding about the whole dynamics. This can also support the design of new control strategies aiming to reduce turbulence levels close to walls (as in Canton *et al.* (2016)), thus leading to drag reduction.

The results presented herein aim to clear the usual complexity related to dealing with the non-linear terms. Even though these may be considered as an external forcing of the system for a simplified analysis, leading for instance to interesting conclusions about linear optimal responses of the system, we must keep in mind that these "forcing" terms come from the dynamics of the flow. Turbulence thus leads to a particular structure, or colour, to these forcing terms, and such structure has been shown to be relevant if one wishes to obtain accurately the flow responses via resolvent analysis. It is notable that for the two considered wavenumbers, at low frequencies, the forcing CSD is of low rank, dominated by its first eigenfunction. Hence, despite the apparent complexity of the bulk of non-linear terms from this flow, order can still be found. Such organisation contributes to the aforementioned constructive or destructive interferences in leading to flow responses. In light of the present results, it is thus relevant to understand and model how coherent structures in turbulent flows give rise to such organised non-linear terms.

Acknowledgements

Petrônio Nogueira was funded by a CNPq scholarship. André Cavalieri acknowledges financial support by CNPq (grant number 310523/2017-6). Pierluigi Morra acknowledge financial support by the European Research Council (ERC) under grant agreement 694452-TRANSEP-ERC-2015-AdG. Direct numerical simulations were performed on resources provided by the Instituto Tecnológico de Aeronáutica and the Swedish National Infrastructure for Computing (SNIC) at NSC, HPC2N and PDC.

Appendix A. Correction due to windowing

The equations shown in the section §2.2 are exact when no windowing function is applied to the turbulent signals; cross-spectral densities (CSD) can be obtained as Fourier transforms of the correlation function. Still, considering most applications, windowing and segment averaging are applied to time series in order to apply Welch's method for a faster determination of cross-spectral densities. As windowing is unavoidable when dealing with large datasets, one can choose the window in order to minimise spectral leakage and/or aliasing. The inclusion of a window in the signal processing, in turn, leads to appearance of new terms in the equations. Following the formulation of Martini *et al.* (2019), the linearised, time-invariant, Navier-stokes equations,

$$\mathbf{H}\frac{\partial\tilde{\mathbf{q}}(t)}{\partial t} = \mathbf{L}\tilde{\mathbf{q}}(t) + \tilde{\mathbf{f}}(t), \tag{21}$$

when multiplied by a window function $h(t)$, can be re-written as

$$\mathbf{H}\frac{\partial(h(t)\tilde{\mathbf{q}}(t))}{\partial t} = \mathbf{L}(h(t)\tilde{\mathbf{q}}(t)) + (h(t)\tilde{\mathbf{f}}(t)) + \mathbf{H}\left(\frac{\partial h}{\partial t}\tilde{\mathbf{q}}\right)(t), \tag{22}$$

where $\tilde{\mathbf{q}} = [\tilde{u}\ \tilde{v}\ \tilde{w}\ \tilde{p}]^T$, $\tilde{\mathbf{f}} = [\tilde{f}_x\ \tilde{f}_y\ \tilde{f}_z\ 0]^T$ are the response and forcing in time domain, and $\mathbf{H}$ is defined to disregard the derivative of the pressure in the equations. The Fourier transform of the windowed signal in each segment is given by

$$\hat{\mathbf{q}}(\omega) = \frac{1}{T}\int_{t_0}^{t_0+T} h(t)\tilde{\mathbf{q}}(t)\mathrm{e}^{\mathrm{i}\omega t}dt, \tag{23}$$

and equivalently for $\mathbf{f}$, where t_0 denotes the initial time for each segment and T the duration of time segments. Defining

$$\overline{\mathbf{q}}(\omega) = \frac{1}{T}\int_{0}^{T} \frac{dh(t)}{dt}\tilde{\mathbf{q}}(t)\mathrm{e}^{\mathrm{i}\omega t}dt, \tag{24}$$

equation 22 can be written as

$$(-\mathrm{i}\omega\mathbf{H} - \mathbf{L})\hat{\mathbf{q}} = \left(\hat{\mathbf{f}} + \mathbf{H}\overline{\mathbf{q}}\right) = \hat{\mathbf{f}}_{corr}, \tag{25}$$

where the right-hand side becomes the effective force of the windowed signal, which is the sum of the external driving force and the external extra term due to windowing. Equation 25 indicates that, even if we manage to obtain converged statistics for the forcing and the response, the fact that we multiply the signal by a window leads to a mismatch between the statistics of the response computed from the velocity fields, and the recovered statistics from the non-linear terms (by using $\mathbf{RPR}^H$). This error is well defined and is a function of the window used in the Welch method, of the operator used in the analysis and of the chosen frequency. Fundamentally the error comes from the difference between $\mathbf{q}$, the

true Fourier transform of the signal, and $\hat{\mathbf{q}}$, its estimate obtained with using the window $h(t)$, the difference also being present for $\mathbf{f}$. Such error is reduced when long segments are taken, which decreases the magnitude of the time derivative of the windowing function in eq. 24; however, the use of sufficiently long segments for negligible correction terms is potentially prohibitive.

Appendix B. Simple coloured forcing statistics

The paper focused on the analysis of the forcing statistics in the minimal Couette flow. From the full forcing statistics, reduced order forcings based on the identification of the relevant parts of the non-linear terms were proposed in order to simplify the analysis. One of the main outcomes of this survey was that coherent structures in the non-linear terms could be clearly distinguished, revealing some of the dynamics behind the streak generation. The results presented herein can also be used to guide modelling of the forcing statistics, since a modelled $\mathbf{P}$ should keep the main characteristics of the one identified in the simulation. To exemplify such a process, we devote this appendix to the analysis of some of the relevant characteristics of $\mathbf{P}$, its effect in $\mathbf{S}$ and how does a simple model for the forcing behave in some frequencies. We start by looking at the frequency studied in the paper ($\omega = 0.0123$) and wavenumbers $(n_\alpha, n_\beta) = (0, 1)$, corresponding to streaks and streamwise vortices studied in section 4.1. The covariance matrices and their respective coherences are shown in figure 16.

As previously observed, the response for this combination of wavenumbers is mostly concentrated at the streamwise direction (leading to a clear signature of streaks), but the other components also have non-negligible amplitudes due to the presence of streamwise vortices in the flow. The forcing also has the same overall behaviour, with higher amplitudes in the streamwise directions and lower in the wall-normal and spanwise ones. Amplitudes of the forcing in the main diagonal of $\mathbf{P}$ are comparable to the ones outside this region, pointing to the presence of coherent structures that extent throughout domain (as in the response). This is confirmed by the coherence computed for each quantity, shown in figure 16(c,d). From these plots, it is clear that both forcing and response are completely coherent throughout the domain (except for the regions where this quantity decays to zero, closer to the walls). For this frequency, it is expected that a model for the forcing that does not consider this high coherence between the components will not adequately represent $\mathbf{P}$, leading thus to errors in predictions of $\mathbf{S}$.

A similar analysis can be performed for a slightly higher frequency still associated with an energetic region of the spectrum ($\omega = 0.135$). Figure 17 shows the same plots for this frequency. As in the case $\omega \to 0$, there is also a dominance of the streamwise component in both $\mathbf{P}$ and $\mathbf{S}$, but the off-diagonal terms are much lower than the ones at the main diagonal of the matrix. Therefore, structures for this case could be assumed as less coherent (or to have a smaller coherence length) than the previous ones. This is seen by the

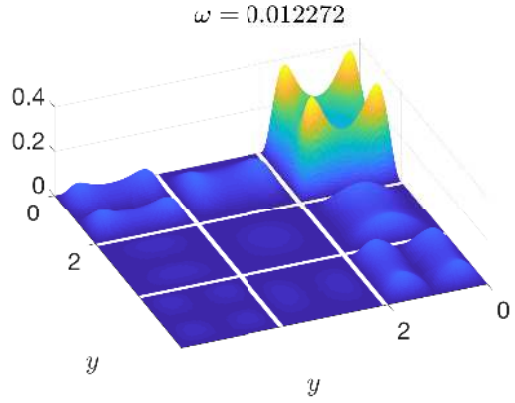

(a) Cross-spectral density matrix of the response

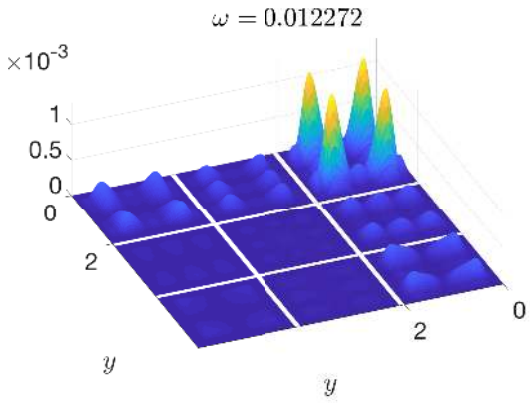

(b) Cross-spectral density matrix of the forcing

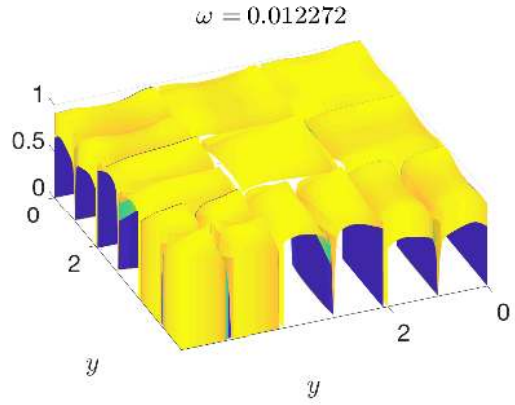

(c) Coherence of the response

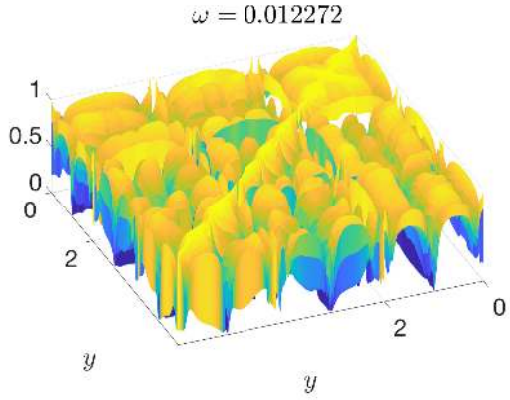

(d) Coherence of the forcing

Figure 16: Cross-spectral density matrix of the response (a) and of the forcing (b) for mode $(0, 1)$ and $\omega = 0.0123$. The coherence of each quantity is shown in (c,d). Each square corresponds to the absolute value of one of the matrix components of the given quantity, starting from the streamwise component (farther from the viewer) to the spanwise component (closer to the viewer).

coherence plots in figure 17(c,d); as usual, the main diagonal has values equal to one, but coherence of both forcing and response decays fast as we move away from that line. Another feature that differentiate this case from the previous one is that the coherence of the cross-components of forcing/velocity for this case is also low. The observed difference between frequencies highlights that the forcing is coloured in time, with different statistics for each frequency. Models based on the white-in-time hypothesis Chevalier *et al.* (2006) would thus be unable to describe the present behaviour.

Consider a simple coloured statistics of the forcing given by the diagonal matrix $\mathbf{P}_{colour} = diag(g_x(y)\ g_y(y)\ g_z(y))$, where $g_{x,y,z}(y)$ are functions that

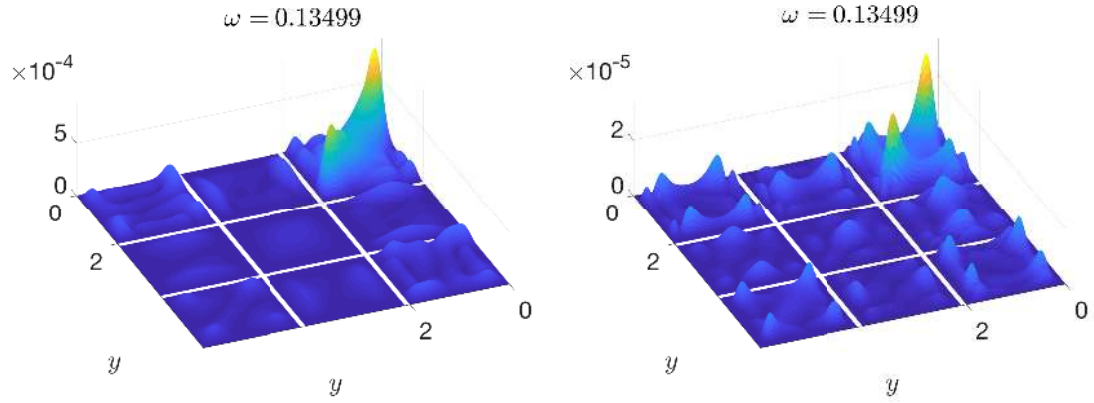

(a) Cross-spectral density matrix of the response

(b) Cross-spectral density matrix of the forcing

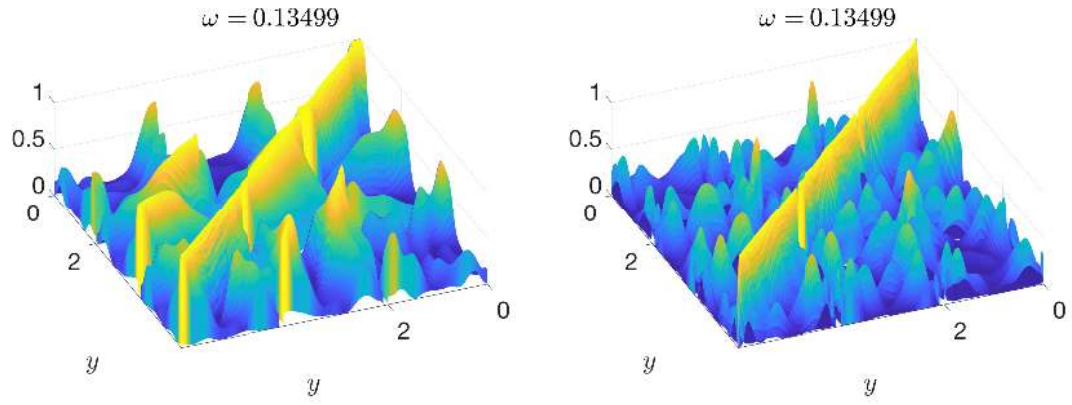

(c) Coherence of the response

(d) Coherence of the forcing

Figure 17: Cross-spectral density matrix of the response (a) and of the forcing (b) for mode $(0, 1)$ and $\omega = 0.135$. The coherence of each quantity is shown in (c,d). Each square corresponds to the absolute value of one of the matrix components of the given quantity, starting from the streamwise component (farther from the viewer) to the spanwise component (closer to the viewer).

satisfy the boundary condition of the problem. These functions can be approximated, for example, by a sum of sine functions in the shape $g_{x,y,z}(y) = |\sum_{n=1}^{N_s} a_{n,x,y,z} \sin n\pi y/2|$, which will lead to real positive values for the main diagonal of $\mathbf{P}$, and zero values at the boundaries. This corresponds to spatially incoherent forcing with amplitude varying in y. An optimisation using the *fminsearch* function in MATLAB using eight sine functions for each $g_{x,y,z}(y)$ (focusing on minimising the error between the predicted $\mathbf{S}$ and the one from DNS) led to forcing statistics whose $\mathbf{S}$ predictions are shown in figure 18. We call these slightly coloured statistics, since only the main diagonal is modelled, and no coherence between cross-components is considered. In figures 18(a,b)

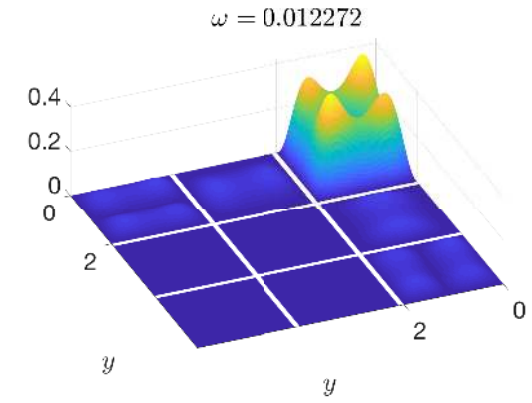

(a) Cross-spectral density matrix of the response (coloured **P**)

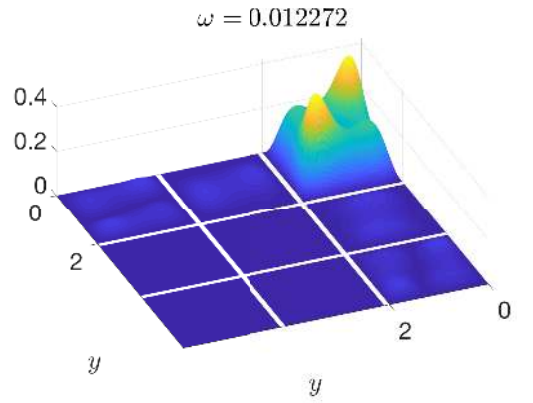

(b) Cross-spectral density matrix of the response (white **P**)

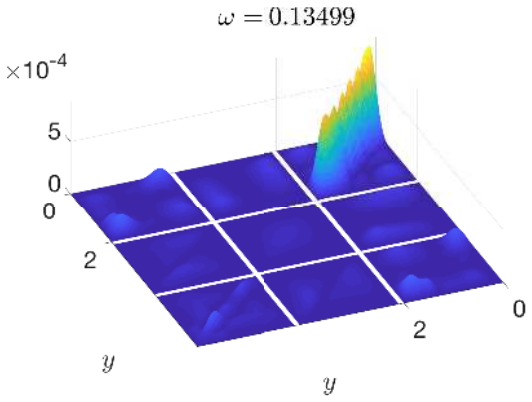

(c) Cross-spectral density matrix of the response (coloured **P**)

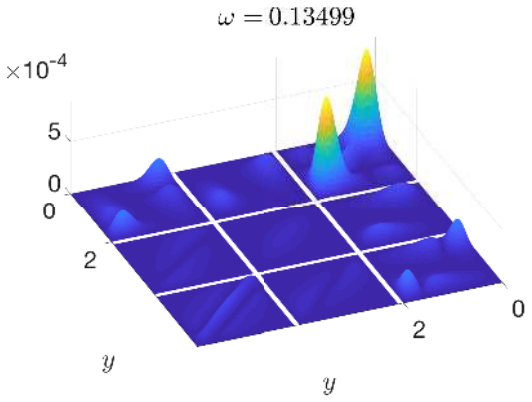

(d) Cross-spectral density matrix of the response (white **P**)

Figure 18: Predicted cross-spectral density matrix of the response using a coloured **P** (a,c) and the white-noise **P** (b,d) for the two frequencies of the study. Each square corresponds to the absolute value of one of the matrix components of the given quantity, starting from the streamwise component (farther from the viewer) to the spanwise component (closer to the viewer).

we compare the results of the prediction using this model and the white-noite forcing statistics. The model seems to improve the results for the streamwise component, improving the amplitudes of the off-diagonal peaks. Still, adding a colour to the forcing in that fashion led to virtually no difference for the other components. Considering that the main problem of the prediction for this frequency is the relative amplitude of the streaks compared to the vortices, as discussed in section 4 this simple model does not seem to be sufficiently accurate to recover accurately the said behaviour.

For higher frequencies ($\omega = 0.135$), the action of the present model is more concentrated in the main diagonal of $\mathbf{S}$, having low influence on the lateral lobes (which are very low for this case). By using the coloured $\mathbf{P}$, we managed to obtain higher amplitudes between the two main peaks of the streamwise component, which qualitatively follows the behaviour found in the data. Considering that the coherence associated with the covariance of the forcing decays sharply from the diagonal for this frequency, the model was expected to work better; still, the present results lack quantitative correspondence. These results point out that simple models for the statistics of the non-linear terms can be useful in order to recover some of the characteristics of the response. However, a more complete description of the statistics of the forcing is required to reproduce results from simulation and experiments when high fidelity levels are needed.

References

Abreu, L. I., Cavalieri, A. V. G., Schlatter, P., Vinuesa, R. & Henningson, D. 2019 Reduced-order models to analyse coherent structures in turbulent pipe flow. In *Turbulence and Shear Flow Phenomena*. Southampton, United Kingdom.

del Álamo, J. C. & Jiménez, J. 2003 Spectra of the very large anisotropic scales in turbulent channels. *Physics of Fluids* **15** (6), L41–L44.

Andersson, P., Brandt, L., Bottaro, A. & Henningson, D. S. 2001 On the breakdown of boundary layer streaks. *Journal of Fluid Mechanics* **428**, 29–60.

Asai, M., Minagawa, M. & Nishioka, M. 2002 The instability and breakdown of a near-wall low-speed streak. *Journal of Fluid Mechanics* **455**, 289–314.

Bodony, D. J. & Lele, S. K. 2008 Current status of jet noise predictions using large-eddy simulation. *AIAA journal* **46** (2), 364.

Brandt, L. 2007 Numerical studies of the instability and breakdown of a boundary-layer low-speed streak. *European Journal of Mechanics-B/Fluids* **26** (1), 64–82.

Butler, K. M. & Farrell, B. F. 1992 Three-dimensional optimal perturbations in viscous shear flow. *Physics of Fluids A: Fluid Dynamics* **4** (8), 1637–1650.

Cabana, M., Fortuné, V. & Jordan, P. 2008 Identifying the radiating core of Lighthill's source term. *Theoretical and Computational Fluid Dynamics* **22** (2), 87–106.

Canton, J., Örlü, R., Chin, C., Hutchins, N., Monty, J. & Schlatter, P. 2016 On large-scale friction control in turbulent wall flow in low Reynolds number channels. *Flow, Turbulence and Combustion* **97** (3), 811–827.

Cavalieri, A., Jordan, P. & Lesshafft, L. 2019 Wave-packet models for jet dynamics and sound radiation. *Applied Mechanics Reviews* .

Cavalieri, A. V. G., Jordan, P., Colonius, T. & Gervais, Y. 2012 Axisymmetric superdirectivity in subsonic jets. *Journal of Fluid Mechanics* **704**, 388.

Chevalier, M., Hœpffner, J., Bewley, T. R. & Henningson, D. S. 2006 State estimation in wall-bounded flow systems. part 2. turbulent flows. *Journal of Fluid Mechanics* **552**, 167–187.

Chevalier, M., Lundbladh, A. & Henningson, D. S. 2007 Simson–a pseudo-spectral solver for incompressible boundary layer flow. *Tech. Rep. TRITA-MEK* .

Cossu, C., Pujals, G. & Depardon, S. 2009 Optimal transient growth and very

large–scale structures in turbulent boundary layers. *Journal of Fluid Mechanics* **619**, 79–94.

Del Alamo, J. C. & Jimenez, J. 2006 Linear energy amplification in turbulent channels. *Journal of Fluid Mechanics* **559**, 205–213.

Ellingsen, T. & Palm, E. 1975 Stability of linear flow. *The Physics of Fluids* **18** (4), 487–488.

Freund, J. B. 2003 Noise-source turbulence statistics and the noise from a Mach 0.9 jet. *Physics of Fluids* **15**, 1788–1799.

Gibson, J. F., Halcrow, J. & Cvitanović, P. 2008 Visualizing the geometry of state space in plane couette flow. *Journal of Fluid Mechanics* **611**, 107–130.

Gustavsson, L. H. 1991 Energy growth of three-dimensional disturbances in plane poiseuille flow. *Journal of Fluid Mechanics* **224**, 241–260.

Hamilton, J. M., Kim, J. & Waleffe, F. 1995 Regeneration mechanisms of near-wall turbulence structures. *Journal of Fluid Mechanics* **287**, 317–348.

Hellström, L. H., Sinha, A. & Smits, A. J. 2011 Visualizing the very-large-scale motions in turbulent pipe flow. *Physics of Fluids* **23** (1), 011703.

Illingworth, S. J., Monty, J. P. & Marusic, I. 2018 Estimating large-scale structures in wall turbulence using linear models. *Journal of Fluid Mechanics* **842**, 146–162.

Jiménez, J. & Pinelli, A. 1999 The autonomous cycle of near-wall turbulence. *Journal of Fluid Mechanics* **389**, 335–359.

Jovanovic, M. R. & Bamieh, B. 2005 Componentwise energy amplification in channel flows. *Journal of Fluid Mechanics* **534**, 145–183.

Kawahara, G., Jimenez, J., Uhlmann, M. & Pinelli, A. 2003 Linear instability of a corrugated vortex sheet–a model for streak instability. *Journal of Fluid Mechanics* **483**, 315–342.

Kline, S. J., Reynolds, W., Schraub, F. & Runstadler, P. 1967 The structure of turbulent boundary layers. *Journal of Fluid Mechanics* **30** (4), 741–773.

Komminaho, J., Lundbladh, A. & Johansson, A. V. 1996 Very large structures in plane turbulent couette flow. *Journal of Fluid Mechanics* **320**, 259–285.

Landahl, M. T. 1980 A note on an algebraic instability of inviscid parallel shear flows. *Journal of Fluid Mechanics* **98** (2), 243–251.

Lee, M. & Moser, R. D. 2018 Extreme-scale motions in turbulent plane couette flows. *Journal of Fluid Mechanics* **842**, 128–145.

Lesshafft, L., Semeraro, O., Jaunet, V., Cavalieri, A. V. G. & Jordan, P. 2019 Resolvent-based modeling of coherent wave packets in a turbulent jet. *Phys. Rev. Fluids* **4**, 063901.

Marsden, J. E. & Chorin, A. J. 1993 *A mathematical introduction to fluid mechanics*. Springer-Verlag.

Martini, E., Cavalieri, A. V., Jordan, P. & Lesshafft, L. 2019 Accurate Frequency Domain Identification of ODEs with Arbitrary Signals. *arXiv preprint arXiv:1907.04787* .

McKeon, B. & Sharma, A. 2010 A critical-layer framework for turbulent pipe flow. *Journal of Fluid Mechanics* **658**, 336–382.

Michalke, A. 1964 On the inviscid instability of the hyperbolic tangent velocity profile. *Journal of Fluid Mechanics* **19** (04), 543–556.

Moarref, R., Sharma, A. S., Tropp, J. A. & McKeon, B. J. 2013 Model-based scaling of the streamwise energy density in high-reynolds-number turbulent channels. *Journal of Fluid Mechanics* **734**, 275–316.

Morra, P., Semeraro, O., Henningson, D. S. & Cossu, C. 2019 On the relevance of reynolds stresses in resolvent analyses of turbulent wall-bounded flows. *Journal of Fluid Mechanics* **867**, 969–984.

Nogueira, P. A., Cavalieri, A. V., Jordan, P. & Jaunet, V. 2019 Large-scale streaky structures in turbulent jets. *Journal of Fluid Mechanics* **873**, 211–237.

Pirozzoli, S., Bernardini, M. & Orlandi, P. 2011 Large-scale motions and inner/outer layer interactions in turbulent couette–poiseuille flows. *Journal of Fluid Mechanics* **680**, 534–563.

Pirozzoli, S., Bernardini, M. & Orlandi, P. 2014 Turbulence statistics in couette flow at high reynolds number. *Journal of Fluid Mechanics* **758**, 327–343.

Pujals, G., García-Villalba, M., Cossu, C. & Depardon, S. 2009 A note on optimal transient growth in turbulent channel flows. *Physics of Fluids* **21** (1), 015109.

Rawat, S., Cossu, C., Hwang, Y. & Rincon, F. 2015 On the self-sustained nature of large-scale motions in turbulent couette flow. *Journal of Fluid Mechanics* **782**, 515–540.

Rosenberg, K. & McKeon, B. J. 2019 Efficient representation of exact coherent states of the navier–stokes equations using resolvent analysis. *Fluid Dynamics Research* **51** (1), 011401.

Schmid, P. J. & Henningson, D. S. 2001 *Stability and Transition in Shear Flows*, *Applied Mathematical Sciences*, vol. 142. Springer, New York, NY.

Schmidt, O. T., Towne, A., Rigas, G., Colonius, T. & Brès, G. A. 2018 Spectral analysis of jet turbulence. *Journal of Fluid Mechanics* **855**, 953–982.

Schoppa, W. & Hussain, F. 1999 Formation of near-wall streamwise vortices by streak instability. In *IUTAM Symposium on Simulation and Identification of Organized Structures in Flows*, pp. 61–78. Springer.

Schoppa, W. & Hussain, F. 2002 Coherent structure generation in near-wall turbulence. *Journal of fluid Mechanics* **453**, 57–108.

Sharma, A. S. & McKeon, B. J. 2013 On coherent structure in wall turbulence. *Journal of Fluid Mechanics* **728**, 196–238.

Smith, T., Moehlis, J. & Holmes, P. 2005 Low-dimensional models for turbulent plane couette flow in a minimal flow unit. *Journal of Fluid Mechanics* **538**, 71–110.

Tammisola, O. & Juniper, M. P. 2016 Coherent structures in a swirl injector at re = 4800 by nonlinear simulations and linear global modes. *Journal of Fluid Mechanics* **792**, 620–657.

Towne, A., Lozano-Durán, A. & Yang, X. 2020 Resolvent-based estimation of space–time flow statistics. *Journal of Fluid Mechanics* **883**, A17.

Towne, A., Schmidt, O. T. & Colonius, T. 2018*a* Spectral proper orthogonal decomposition and its relationship to dynamic mode decomposition and resolvent analysis. *Journal of Fluid Mechanics* **847**, 821–867.

Towne, A., Yang, X. & Lozano-Durán, A. 2018*b* Approximating space-time flow statistics from a limited set of known correlations. In *2018 Fluid Dynamics Conference*, p. 4043.

Towne, A. S. 2016 Advancements in jet turbulence and noise modeling: accurate one-way solutions and empirical evaluation of the nonlinear forcing of wavepackets. PhD thesis, California Institute of Technology.

Trefethen, L. N. 2000 *Spectral methods in MATLAB*, , vol. 10. Society for Industrial Mathematics.

Tsukahara, T., Kawamura, H. & Shingai, K. 2006 Dns of turbulent couette flow with emphasis on the large-scale structure in the core region. *Journal of Turbulence* **7**, N19.

Waleffe, F. 1997 On a self-sustaining process in shear flows. *Physics of Fluids* **9** (4), 883–900.

Zare, A., Jovanović, M. R. & Georgiou, T. T. 2017 Colour of turbulence. *Journal of Fluid Mechanics* **812**, 636–680.